Downloaded from orbit.dtu.dk on: May 05, 2023

DTU Library

Disintegration of beech wood char during thermal conversion

Hindsgaul, Claus

Publication date:
2007

Document Version
Publisher's PDF, also known as Version of record

Link back to DTU Orbit

Citation (APA):
Hindsgaul, C. (2007). *Disintegration of beech wood char during thermal conversion*. Technical University of Denmark.

General rights
Copyright and moral rights for the publications made accessible in the public portal are retained by the authors and/or other copyright owners and it is a condition of accessing publications that users recognise and abide by the legal requirements associated with these rights.

- Users may download and print one copy of any publication from the public portal for the purpose of private study or research.
- You may not further distribute the material or use it for any profit-making activity or commercial gain
- You may freely distribute the URL identifying the publication in the public portal

If you believe that this document breaches copyright please contact us providing details, and we will remove access to the work immediately and investigate your claim.

MEK–ET–PHD–2006–02

Disintegration of beech wood char during thermal conversion

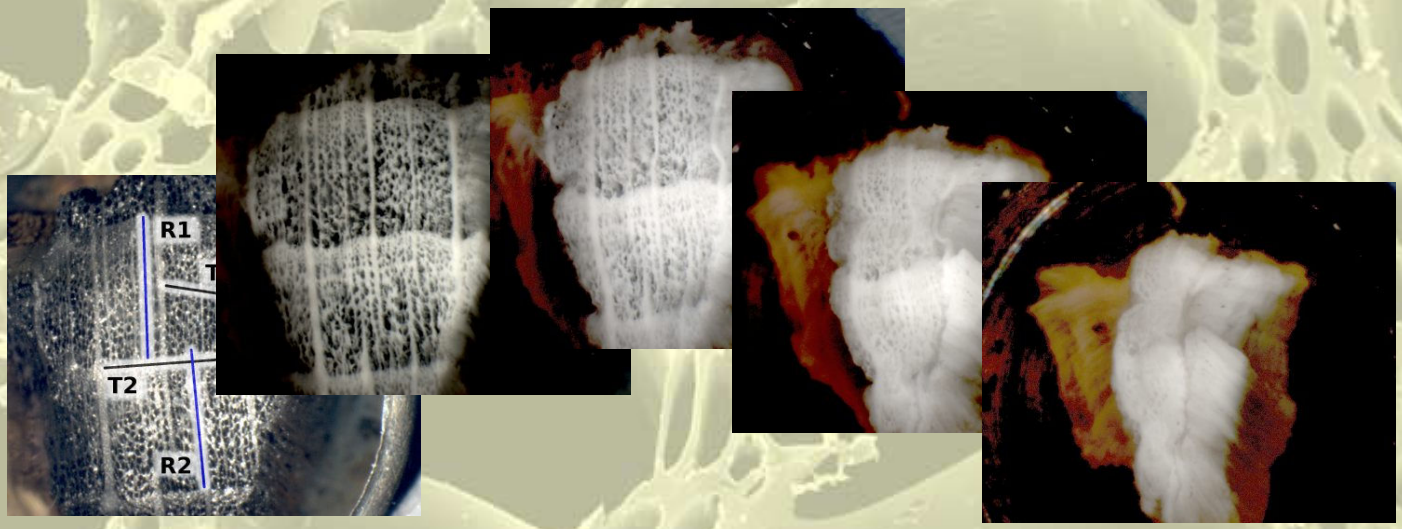

Appendix

Ph.D. Thesis
Claus Hindsgaul

Department of Mechanical Engineering
Department of Chemical Engineering
Technical University of Denmark (DTU)

August 2006

CHEC

MEK

A. Diffusion measurements

The following table present the raw data from diffusion measurement results in longitudinal (sample name starts with an "L"), radial (sample name starts with an "R") and tangential (sample name starts with an "T") directions as well as the reference specimen "Test2" (see Section 2.3.3). "Test2x" is the Test2 reference specimen after exposure to SO_2, which formed cracks in the sample and apparently altered the effective diffusion coefficient.

The sorting order is: sample direction, degree of conversion, gas pair and gas flow.

			Measured data				*Calculated from measured data*				
Sample	**Conv**	**Gas pair**	$x_{A\delta}$	x_{B0}	$F_{A,in}$	$F_{B,in}$	$D_{eff,A}$	$D_{eff,B}$	$\frac{D_{eff,A}}{\mathcal{D}_{AB}}$	$\frac{D_{eff,B}}{\mathcal{D}_{AB}}$	$\frac{D_{eff,A}}{D_{eff,B}}$
	[-]	A-B	[ppm]	[ppm]	[l/min]	[l/min]	[m^2/s]	[m^2/s]	[-]	[-]	[-]
L4	0.00	N2-CO	-	5100	1.026	1.013	-	1.04E-5	-	4.87E-1	-
L4	0.00	N2-CO	-	10250	0.505	0.501	-	1.03E-5	-	4.81E-1	-
L4	0.00	CO2-CO	4522	5464	0.780	0.780	7.95E-6	7.67E-6	4.84E-1	4.68E-1	1.04
L4	0.00	CO2-CO	3525	5514	0.780	1.029	8.16E-6	7.74E-6	4.98E-1	4.72E-1	1.06
L5-1	0.12	N2-CO	-	8750	0.502	0.502	-	1.03E-5	-	4.83E-1	-
L5-1	0.12	N2-CO	-	8300	0.531	0.503	-	1.04E-5	-	4.85E-1	-
L5-1	0.12	CO2-CO	3325	4250	0.769	1.021	9.03E-6	6.93E-6	5.51E-1	4.23E-1	1.30
R1-3	0.00	NO-CO	65	62	0.497	0.499	2.48E-8	2.27E-8	1.16E-3	1.06E-3	1.09
R1-3	0.00	NO-CO	39	47	0.999	0.998	2.97E-8	3.46E-8	1.39E-3	1.62E-3	0.86
R1-3	0.00	NO-CO	76	87	0.499	0.498	2.89E-8	3.20E-8	1.35E-3	1.49E-3	0.90
R1-3	0.00	NO-CO	31	29	1.010	1.010	2.42E-8	2.17E-8	1.13E-3	1.01E-3	1.11
R1-3	0.00	N2-CO	-	55	0.497	0.499	-	2.05E-8	-	9.56E-4	-
R1-3	0.00	CO2-N2	128	-	0.506	0.501	5.39E-8	-	3.25E-3	-	-
R1-3	0.00	CO2-CO	166	62	0.507	0.493	6.87E-8	2.10E-8	4.19E-3	1.28E-3	3.27
R1-3	0.00	CO2-CO	49	69	0.506	0.500	2.06E-8	2.34E-8	1.26E-3	1.43E-3	0.88
R1-3	0.00	CO2-CO	95	74	0.505	0.500	3.99E-8	2.51E-8	2.43E-3	1.53E-3	1.59
R1-3	0.00	CO2-CO	73	33	0.999	1.000	6.14E-8	2.20E-8	3.74E-3	1.34E-3	2.79
R5	0.00	NO-CO	106	105	0.500	0.499	3.07E-8	2.94E-8	1.43E-3	1.37E-3	1.04
R5	0.00	NO-CO	213	219	0.250	0.258	3.19E-8	3.07E-8	1.49E-3	1.43E-3	1.04
R5	0.00	N2-CO	-	102	0.509	0.498	-	2.96E-8	-	1.38E-3	-
R5	0.00	CO2-CO	235	103	0.400	0.508	7.62E-8	2.10E-8	4.65E-3	1.28E-3	3.62
R5	0.00	CO2-CO	493	196	0.208	0.251	7.91E-8	2.08E-8	4.82E-3	1.27E-3	3.81
R7-1	0.18	NO-CO	342	382	0.253	0.256	1.20E-7	1.28E-7	5.61E-3	5.99E-3	0.94
R7-1	0.18	N2-CO	-	234	0.502	0.503	-	1.58E-7	-	7.40E-3	-
R7-1	0.18	N2-CO	-	462	0.253	0.256	-	1.58E-7	-	7.36E-3	-
R7-1	0.18	CO2-CO	997	311	0.204	0.253	3.83E-7	7.67E-8	2.33E-2	4.68E-3	4.99

Sample	Conv	Gas pair	$x_{A\delta}$	x_{B0}	$F_{A,in}$	$F_{B,in}$	$D_{eff,A}$	$D_{eff,B}$	$\frac{D_{eff,A}}{\mathcal{D}_{AB}}$	$\frac{D_{eff,B}}{\mathcal{D}_{AB}}$	$\frac{D_{eff,A}}{D_{eff,B}}$
	[-]	A-B	[ppm]	[ppm]	[l/min]	[l/min]	[m^2/s]	[m^2/s]	[-]	[-]	[-]
R7-1	0.18	CO2-CO	487	158	0.402	0.501	3.70E-7	7.67E-8	2.25E-2	4.68E-3	4.82
R3-1	0.46	NO-CO	1522	1672	1.006	1.002	2.16E-6	2.31E-6	1.01E-1	1.08E-1	0.94
R3-1	0.46	N2-CO	-	1595	1.006	0.999	-	2.23E-6	-	1.04E-1	-
R3-1	0.46	CO2-CO	3018	-	0.397	0.503	2.39E-6	-	1.45E-1	-	-
R3-1	0.46	CO2-CO	1531	1619	0.782	0.997	2.39E-6	1.58E-6	1.46E-1	9.64E-2	1.51
R3-1	0.46	CO2-CO	1497	1269	1.008	1.003	2.35E-6	1.60E-6	1.43E-1	9.73E-2	1.47
R2	0.50	NO-CO	1233	1441	0.998	0.997	2.35E-6	2.66E-6	1.10E-1	1.24E-1	0.88
R2	0.50	N2-CO	-	1375	1.009	1.011	-	2.61E-6	-	1.22E-1	-
R2	0.50	CO2-CO	1245	1354	0.800	1.016	2.67E-6	1.83E-6	1.63E-1	1.11E-1	1.46
T5	0.00	NO-CO	52	105	0.251	0.252	8.60E-9	1.67E-8	4.02E-4	7.81E-4	0.52
T5	0.00	NO-CO	67	108	0.260	0.253	1.11E-8	1.78E-8	5.18E-4	8.32E-4	0.62
T5	0.00	NO-CO	35	53	0.502	0.502	1.16E-8	1.67E-8	5.40E-4	7.82E-4	0.69
T5	0.00	N2-CO	-	35	0.502	0.502	-	1.13E-8	-	5.29E-4	-
T5	0.00	N2-CO	-	92	0.258	0.255	-	1.53E-8	-	7.17E-4	-
T5	0.00	CO2-CO	41	54	0.389	0.506	1.50E-8	1.21E-8	9.14E-4	7.39E-4	1.24
T5	0.00	CO2-CO	105	103	0.197	0.253	1.92E-8	1.17E-8	1.17E-3	7.13E-4	1.64
T11	0.20	NO-CO	376	412	0.252	0.246	4.95E-8	5.36E-8	2.31E-3	2.50E-3	0.92
T11	0.20	NO-CO	376	398	0.254	0.250	5.03E-8	5.23E-8	2.35E-3	2.44E-3	0.96
T11	0.20	NO-CO	1163	1197	0.081	0.077	4.82E-8	5.01E-8	2.25E-3	2.34E-3	0.96
T11	0.20	N2-CO	-	408	0.252	0.246	-	5.39E-8	-	2.52E-3	-
T11	0.20	N2-CO	-	389	0.256	0.250	-	5.23E-8	-	2.44E-3	-
T11	0.20	CO2-CO	956	691	0.103	0.105	5.90E-8	3.35E-8	3.60E-3	2.04E-3	1.76
T11	0.20	CO2-CO	198	140	0.501	0.505	5.90E-8	3.30E-8	3.60E-3	2.01E-3	1.79
T11	0.20	CO2-CO	387	281	0.251	0.258	5.89E-8	3.32E-8	3.59E-3	2.02E-3	1.77
T3	0.48	NO-CO	1264	1397	0.536	0.498	7.07E-7	8.14E-7	3.31E-2	3.80E-2	0.87
T3	0.48	N2-CO	-	1365	0.538	0.500	-	8.10E-7	-	3.78E-2	-
T3	0.48	CO2-CO	1524	1459	0.393	0.502	9.49E-7	5.67E-7	5.78E-2	3.46E-2	1.67
T4	0.53	NO-CO	-	1405	0.500	0.500	-	1.04E-6	-	4.86E-2	-
T4	0.53	NO-CO	1505	1561	0.535	0.506	1.17E-6	1.24E-6	5.45E-2	5.78E-2	0.94
T4	0.53	N2-CO	-	1650	0.499	0.503	-	1.24E-6	-	5.78E-2	-
T4	0.53	CO2-N2	1990	-	0.495	0.494	1.66E-6	-	1.00E-1	-	-
T4	0.53	CO2-N2	977	-	1.002	1.000	1.65E-6	-	9.94E-2	-	-
T4	0.53	CO2-CO	1802	1281	0.500	0.500	1.52E-6	8.63E-7	9.29E-2	5.26E-2	1.77
T4	0.53	CO2-CO	955	623	1.012	1.001	1.61E-6	8.48E-7	9.84E-2	5.17E-2	1.90
T4	0.53	CO2-CO	1980	1257	0.495	0.498	1.67E-6	8.39E-7	1.02E-1	5.12E-2	1.99
T4	0.53	CO2-CO	-	1235	0.503	0.501	-	8.36E-7	-	5.10E-2	-
Test2	0.00	NO-CO	1306	1337	0.500	0.498	1.76E-7	1.75E-7	8.23E-3	8.17E-3	1.01
Test2	0.00	N2-SO2	-	1094	0.506	0.530	-	1.82E-7	-	1.42E-2	-
Test2	0.00	N2-SO2	-	1896	0.262	0.246	-	1.64E-7	-	1.28E-2	-
Test2	0.00	N2-SO2	-	1946	0.262	0.214	-	1.68E-7	-	1.32E-2	-
Test2	0.00	N2-SO2	-	564	1.000	1.000	-	1.86E-7	-	1.45E-2	-

Sample	Conv	Gas pair	$x_{A\delta}$	x_{B0}	$F_{A,in}$	$F_{B,in}$	$D_{eff,A}$	$D_{eff,B}$	$\frac{D_{eff,A}}{\mathcal{D}_{AB}}$	$\frac{D_{eff,B}}{\mathcal{D}_{AB}}$	$\frac{D_{eff,A}}{D_{eff,B}}$
	[-]	A-B	[ppm]	[ppm]	[l/min]	[l/min]	[m^2/s]	[m^2/s]	[-]	[-]	[-]
Test2	0.00	N2-SO2	-	1048	0.508	0.497	-	1.76E-7	-	1.37E-2	-
Test2	0.00	N2-CO	-	1315	0.499	0.498	-	1.74E-7	-	8.13E-3	-
Test2	0.00	N2-CO	-	1460	0.500	0.505	-	1.94E-7	-	9.05E-3	-
Test2	0.00	N2-CO	-	1310	0.501	0.497	-	1.74E-7	-	8.13E-3	-
Test2	0.00	CO2-SO2	-	720	0.502	0.499	-	1.06E-7	-	1.32E-2	-
Test2	0.00	CO2-SO2	-	1456	0.254	0.259	-	1.08E-7	-	1.35E-2	-
Test2	0.00	CO2-N2	1252	-	0.504	0.509	1.90E-7	-	1.15E-2	-	-
Test2	0.00	CO2-N2	1371	-	0.500	0.500	2.05E-7	-	1.23E-2	-	-
Test2	0.00	CO2-CO	2453	1871	0.253	0.257	1.89E-7	1.13E-7	1.15E-2	6.88E-3	1.67
Test2	0.00	CO2-CO	1278	946	0.507	0.508	1.94E-7	1.14E-7	1.18E-2	6.96E-3	1.70
Test2	0.00	CO2-CO	1378	709	0.500	0.498	2.05E-7	8.43E-8	1.25E-2	5.14E-3	2.43
Test2	0.00	CO2-CO	1323	709	0.499	0.497	1.96E-7	8.41E-8	1.20E-2	5.13E-3	2.33
Test2	0.00	CO2-CO	644	471	1.012	1.008	1.93E-7	1.13E-7	1.18E-2	6.91E-3	1.71
Test2	0.00	CO2-CO	705	354	0.983	1.009	2.12E-7	8.26E-8	1.29E-2	5.04E-3	2.57
Test2	0.00	CO2-CO	1321	934	0.398	0.500	1.97E-7	8.84E-8	1.20E-2	5.39E-3	2.23
Test2	0.00	CO2-CO	638	479	0.801	1.009	1.92E-7	9.12E-8	1.17E-2	5.56E-3	2.10
Test2x	0.00	CO2-N2	2301	-	0.257	0.239	1.65E-7	-	9.93E-3	-	-
Test2x	0.00	CO2-N2	2281	-	0.257	0.239	1.63E-7	-	9.84E-3	-	-
Test2x	0.00	CO2-N2	360	-	0.254	0.249	1.50E-7	-	9.01E-3	-	-
Test2x	0.00	CO2-N2	1094	-	0.506	0.507	1.66E-7	-	9.97E-3	-	-
Test2x	0.00	CO2-N2	1103	-	0.506	0.507	1.67E-7	-	1.01E-2	-	-
Test2x	0.00	CO2-N2	96	-	0.504	0.496	1.57E-7	-	9.45E-3	-	-
Test2x	0.00	CO2-CO	2280	1771	0.264	0.247	1.69E-7	1.12E-7	1.03E-2	6.80E-3	1.51
Test2x	0.00	CO2-CO	2279	1766	0.262	0.248	1.69E-7	1.10E-7	1.03E-2	6.71E-3	1.54
Test2x	0.00	CO2-CO	2304	1791	0.257	0.248	1.71E-7	1.10E-7	1.04E-2	6.69E-3	1.56
Test2x	0.00	CO2-CO	563	466	1.007	1.016	1.70E-7	1.12E-7	1.04E-2	6.80E-3	1.53
Test2x	0.00	CO2-CO	1164	926	0.511	0.499	1.73E-7	1.12E-7	1.06E-2	6.86E-3	1.54
Test2x	0.00	CO2-CO	1143	926	0.507	0.500	1.70E-7	1.12E-7	1.04E-2	6.81E-3	1.53

B. Permeability measurements

The following tables present the raw data from permeability measurements in longitudinal (sample name starts with an "L"), radial (sample name starts with an "R") and tangential (sample name starts with an "T") directions as well as the reference specimen "Test2" (see Section 2.3.3). The sorting order is: sample direction, degree of conversion, gas and gas flow.

Sample	**Conv** [-]	**Gas**	*Measured data* ΔP [Pa]	F [ml/min]	*Calculated from measured* **Permeability,** Φ [mD]
L4	0.00	N2	20.2	10.2	17,982.25
L4	0.00	N2	41.7	21.8	18,623.82
L4	0.00	N2	66.9	35.5	18,866.24
L4	0.00	N2	88.1	46.5	18,798.08
L4	0.00	N2	109.0	58.1	18,957.49
L4	0.00	N2	159.0	84.2	18,845.73
L4	0.00	N2	334.0	177.1	18,853.65
L4	0.00	N2	659.0	355.7	19,161.39
L4	0.00	N2	1,590.0	863.0	19,180.42
L1	0.10	CO2	5.7	6.4	15,818.25
L1	0.10	CO2	17.5	19.9	15,893.54
L1	0.10	CO2	36.4	40.9	15,767.13
L1	0.10	N2	2.8	2.7	16,225.35
L1	0.10	N2	6.0	5.6	15,705.93
L1	0.10	N2	10.7	10.1	15,708.69
L1	0.10	N2	14.2	13.5	15,837.08
L1	0.10	N2	25.3	23.9	15,795.57
L1	0.10	N2	43.9	41.8	15,902.40
L1	0.10	N2	74.9	71.2	15,868.74
L1	0.10	N2	132.1	125.9	15,914.34
L1	0.10	N2	199.4	189.8	15,888.86
L1	0.10	N2	256.9	244.6	15,888.79
L1	0.10	N2	318.1	302.9	15,885.58
L1	0.10	N2	394.7	377.4	15,945.51
L1	0.10	N2	472.0	449.9	15,889.58
L1	0.10	N2	623.6	593.7	15,858.98
L1	0.10	N2	778.0	740.5	15,842.73
L1	0.10	N2	930.7	883.6	15,790.82
L1	0.10	N2	1,085.7	1026.0	15,706.01
L1	0.10	N2	1,243.0	1173.0	15,671.84

Sample	**Conv** [-]	**Gas**	ΔP [Pa]	F [ml/min]	**Permeability,** Φ [mD]
L1	0.10	N2	1,401.5	1325.0	15,688.39
L1	0.10	N2	1,568.7	1482.0	15,664.20
L2	0.10	N2	2.3	1.5	14,729.64
L2	0.10	N2	8.3	5.6	15,326.44
L2	0.10	N2	16.9	11.4	15,268.41
L2	0.10	N2	41.5	28.1	15,362.17
L2	0.10	N2	84.9	57.6	15,372.92
L2	0.10	N2	252.4	171.4	15,379.96
L2	0.10	N2	979.4	659.2	15,189.29
L2	0.10	N2	1,466.9	981.4	15,062.17
L3	0.10	N2	35.4	11.5	16,163.95
L3	0.10	N2	71.4	23.0	16,116.25
L3	0.10	N2	97.0	31.3	16,141.38
L5-1	0.12	N2	17.2	6.3	15,341.73
L5-1	0.12	N2	47.1	18.5	16,532.32
L5-1	0.12	N2	76.3	28.6	15,788.78
L5-1	0.12	N2	91.0	34.8	16,092.07
L5-1	0.12	N2	254.0	96.3	15,950.24
L5-1	0.12	N2	460.0	177.6	16,226.28
L5-1	0.12	N2	887.0	346.6	16,388.03
L5-1	0.12	N2	2,172.0	858.9	16,480.54
L5-1	0.12	N2	4,521.0	1748.0	15,931.01
R5	0.00	N2	8,050.0	0.2	0.29
R5	0.00	N2	68,000.0	2.1	0.24
R5	0.00	N2	98,000.0	3.5	0.25
R5	0.00	N2	160,000.0	6.8	0.24
R7-1	0.18	CO2	11,275.0	0.5	0.86
R7-1	0.18	CO2	15,570.0	0.6	0.78
R7-1	0.18	CO2	17,616.0	0.9	0.90
R7-1	0.18	CO2	102,000.0	8.2	1.08
R7-1	0.18	CO2	130,000.0	11.1	1.05
R7-1	0.18	N2	19,090.0	1.3	1.55
R7-1	0.18	N2	85,000.0	5.7	1.14
R7-1	0.18	N2	118,000.0	8.6	1.11
R3-1	0.46	N2	235.0	1.5	154.45
R3-1	0.46	N2	10,000.0	60.0	142.32
R2	0.50	CO2	155.0	0.7	126.23
R2	0.50	CO2	87,000.0	383.6	86.91
R2	0.50	CO2	115,000.0	506.5	79.16
R2	0.50	N2	126.0	0.6	173.06
R2	0.50	N2	235.0	1.5	208.63

Sample	**Conv** [-]	**Gas**	ΔP [Pa]	F [ml/min]	**Permeability,** Φ [mD]
R2	0.50	N2	269.0	1.5	183.73
R2	0.50	N2	78,000.0	353.2	109.93
R2	0.50	N2	117,000.0	524.2	95.50
R2	0.50	N2	152,000.0	695.4	87.89
T1	0.00	CO	103,000.0	10.7	0.75
T1	0.00	CO	109,000.0	11.3	0.74
T1	0.00	CO2	103,000.0	10.7	0.64
T1	0.00	CO2	99,000.0	11.2	0.70
T1	0.00	CO2	109,000.0	11.3	0.63
T1	0.00	CO2	169,000.0	22.1	0.66
T1	0.00	N2	59,000.0	5.1	0.74
T1	0.00	N2	101,000.0	10.3	0.75
T1	0.00	N2	138,000.0	15.3	0.73
T5	0.00	N2	6,045.0	0.4	0.78
T5	0.00	N2	70,000.0	5.7	0.70
T5	0.00	N2	120,000.0	11.6	0.70
T11	0.20	N2	13,040.0	1.3	0.89
T11	0.20	N2	17,180.0	1.8	0.88
T11	0.20	N2	91,000.0	11.4	0.81
T11	0.20	N2	122,000.0	17.0	0.82
T4	0.53	N2	300.0	0.3	26.21
T4	0.53	N2	50,000.0	50.7	21.84
T4	0.53	N2	105,000.0	103.0	17.37
Test2	0.00	CO	0.8	2.2	13,120.08
Test2	0.00	CO	2.1	5.7	12,709.96
Test2	0.00	CO	10.8	28.4	12,406.65
Test2	0.00	CO	22.0	56.3	12,070.95
Test2	0.00	CO2	0.4	1.5	14,483.07
Test2	0.00	CO2	1.2	3.9	12,864.95
Test2	0.00	CO2	6.7	20.4	12,114.38
Test2	0.00	CO2	13.3	39.5	11,828.15
Test2	0.00	N2	0.3	0.7	11,316.34
Test2	0.00	N2	0.7	1.5	10,065.98
Test2	0.00	N2	0.9	2.0	10,424.72
Test2	0.00	N2	1.1	2.8	12,042.90
Test2	0.00	N2	2.3	5.7	11,746.31
Test2	0.00	N2	4.8	11.5	11,365.55
Test2	0.00	N2	10.0	24.5	11,637.07
Test2	0.00	N2	19.7	47.7	11,495.61
Test2	0.00	N2	24.3	58.9	11,503.54
Test2	0.00	N2	71.1	166.8	11,135.15
Test2	0.00	N2	99.5	232.5	11,089.41

C. W-K calculations

This appendix documents the derivations of the expressions used to calculate diffusion coefficients and Knudsen constants from the experimental measurements on the Wicke-Kallenbach cell.

C.1. The diffusive flux

In order to calculate the diffusion coefficients from the diffusion measurements, the diffusive fluxes, $F_{0,out}$ and $F_{\delta,out}$ was determined. A mass balance for chamber A in Figure 2.1 gives:

$$F_{0,out} = F_{i,in} - F_i + F_j \tag{C.1}$$

$$\Leftrightarrow x_{j0} = \frac{F_j}{F_{0,out}} = \frac{F_j}{F_{i,in} - F_i + F_j} \tag{C.2}$$

$$\Leftrightarrow F_i = F_j - \frac{F_j}{x_{j0}} + F_{i,in} = -\left(\frac{1}{x_{j0}} - 1\right) F_j + F_{i,in} \tag{C.3}$$

$$\Leftrightarrow F_j = \frac{F_{i,in} - F_i}{\frac{1}{x_{j0}} - 1} = \frac{F_{i,in} - F_i}{\alpha_j} \tag{C.4}$$

where $\alpha_j = \frac{1}{x_{j0}} - 1$. Similarly, a mass balance for chamber B gives:

$$F_i = \frac{F_{j,in} - F_j}{\alpha_i} \tag{C.5}$$

where $\alpha_i = \frac{1}{x_{i\delta}} - 1$. Inserting (C.4) in (C.5):

$$F_i = \frac{F_{j,in} - \frac{F_{i,in} - F_i}{\alpha_j}}{\alpha_i} \tag{C.6}$$

$$= \frac{\alpha_j F_{j,in} - F_{i,in} + F_i}{\alpha_i \alpha_j} \tag{C.7}$$

$$\Leftrightarrow F_i \cdot \left(1 - \frac{1}{\alpha_i \alpha_j}\right) = \frac{\alpha_j F_{j,in} - F_{i,in}}{\alpha_i \alpha_j} \tag{C.8}$$

$$\Leftrightarrow F_i = \frac{\alpha_j F_{j,in} - F_{i,in}}{\left(1 - \frac{1}{\alpha_i \alpha_j}\right) \alpha_i \alpha_j} \tag{C.9}$$

$$= \frac{F_{i,in} - \alpha_j F_{j,in}}{1 - \alpha_i \alpha_j} \tag{C.10}$$

A similar expression was found for F_j by inserting (C.5) in (C.4). In summary, the diffusive flows can be found from the gas concentrations $x_{i\delta}$ and x_{j0} and the inlet flows $F_{i,in}$ and $F_{j,in}$ using the following formulas:

$$F_i = \frac{F_{i,in} - \alpha_j F_{j,in}}{1 - \alpha_i \alpha_j} \tag{C.11}$$

$$F_j = \frac{F_{j,in} - \alpha_i F_{i,in}}{1 - \alpha_i \alpha_j} \tag{C.12}$$

where:

$$\alpha_i = \frac{1}{x_{i\delta}} - 1 = \frac{1 - x_{i\delta}}{x_{i\delta}} \tag{C.13}$$

$$\alpha_j = \frac{1}{x_{j0}} - 1 = \frac{1 - x_{j0}}{x_{j0}} \tag{C.14}$$

In some cases only one of $x_{i\delta}$ or x_{j0} could be measured (when using N_2 as one gas or one concentration was outside the gas analyser range). In these cases Grahams law was used to determine the diffusive flux of the opposite gas:

$$F_j = \sqrt{\frac{M_i}{M_j}} F_i \tag{C.15}$$

A total mass balance for chamber B:

$$F_{\delta,out} = F_{j,in} + F_j - F_i = F_{j,in} + \left(\sqrt{\frac{M_i}{M_j}} - 1\right) F_i \tag{C.16}$$

A mass balance of gas species i in chamber B:

$$F_i = F_{\delta,out}\, x_{i\delta} = \left[F_{j,in} + \left(\sqrt{\frac{M_i}{M_j}} - 1\right) F_i\right] x_{i\delta} \tag{C.17}$$

$$\Leftrightarrow F_{j,in} = F_i \left[\frac{1}{x_{i\delta}} - \left(\sqrt{\frac{M_i}{M_j}} - 1\right)\right] \tag{C.18}$$

$$\Leftrightarrow F_i = \frac{F_{j,in}}{\frac{1}{x_{i\delta}} + 1 - \sqrt{\frac{M_i}{M_j}}} \tag{C.19}$$

C.2. Finding $\mathcal{D}_{eff}$

When the two molar fluxes was found, the effective binary diffusion coefficient for the gas pair i-j, $\mathcal{D}_{eff,ij}$, could be derived.

The Dusty Gas Model (1.57) was used to describe the concentration gradient through the sample. For the binary system of species i and j ($x_i = 1 - x_j$) in the sample, (1.57) becomes:

$$\begin{aligned}
-\nabla C_i &= \frac{x_j \vec{J}_i - x_i \vec{J}_j}{\mathcal{D}_{eff,ij}} + \frac{\vec{J}_i}{D_{eff,K,i}} + \frac{x_i \left(\frac{C_t \vec{\Phi}}{\mu}\right) \nabla p}{D_{eff,K,i}} \\
&= \frac{(1-x_i)\vec{J}_i - x_i \vec{J}_j}{\mathcal{D}_{eff,ij}} + \frac{\vec{J}_i}{D_{eff,K,i}} + \frac{x_i}{D_{eff,K,i}} \left(\frac{C_t \vec{\Phi}}{\mu}\right) \nabla p \\
&= \frac{1 - x_i \cdot \left(1 + \frac{\vec{J}_j}{\vec{J}_i}\right)}{\mathcal{D}_{eff,ij}} \vec{J}_i + \frac{\vec{J}_i}{D_{eff,K,i}} + \frac{x_i}{D_{eff,K,i}} \left(\frac{C_t \vec{\Phi}}{\mu}\right) \nabla p \\
&= \vec{J}_i \cdot \left[\frac{1 - x_i \cdot \left(1 + \frac{\vec{J}_j}{\vec{J}_i}\right)}{\mathcal{D}_{eff,ij}} + \frac{1}{D_{eff,K,i}}\right] + \frac{x_i}{D_{eff,K,i}} \left(\frac{C_t \vec{\Phi}}{\mu}\right) \nabla p
\end{aligned} \tag{C.20}$$

$$\begin{aligned}
\Leftrightarrow \vec{J}_i &= \frac{-\nabla C_i - \frac{x_i}{D_{eff,K,i}} \left(\frac{C_t \vec{\Phi}}{\mu}\right) \nabla p}{\frac{1 - x_i \cdot \left(1 + \frac{\vec{J}_j}{\vec{J}_i}\right)}{\mathcal{D}_{eff,ij}} + \frac{1}{D_{eff,K,i}}} \\
&= -D_{eff,i} \nabla C_i - \frac{D_{eff,i}}{D_{eff,K,i}} \left(\frac{C_t \vec{\Phi}}{\mu}\right) x_i \nabla p
\end{aligned} \tag{C.21}$$

where

$$D_{eff,i} = \left(\frac{1 - x_i \cdot \left(1 + \frac{\vec{J}_j}{\vec{J}_i}\right)}{\mathcal{D}_{eff,ij}} + \frac{1}{D_{eff,K,i}}\right)^{-1} \tag{C.22}$$

For steady-state one-dimensional diffusion through the sample (length δ) without accumulation of gases, J_i and J_j must be constant throughout the medium. That is, $\frac{\partial J_i}{\partial \xi} = 0$. For no pressure gradient ($\nabla p = 0$):

$$\int_{\xi=0}^{\delta} J_i \partial \xi = \delta J_i = \int_{\xi=0}^{\delta} -D_{eff,i} \frac{\partial C_i}{\partial \xi} \partial \xi \tag{C.23}$$

$$= \int_{C_i=C_{i0}}^{C_{i\delta}} -D_{eff,i}\,\partial C_i \tag{C.24}$$

$$= -C_t \int_{x_i=x_{i0}}^{x_{i\delta}} D_{eff,i}\,\partial x_i \tag{C.25}$$

$$= -C_t \int_{x_i=x_{i0}}^{x_{i\delta}} \left(\frac{1 - x_i \cdot \left(1 + \frac{J_j}{J_i}\right)}{\mathcal{D}_{eff,ij}} + \frac{1}{D_{eff,K,i}} \right)^{-1} \partial x_i \tag{C.26}$$

For $J_i \neq -J_j$ an integration variable $u = \left(\frac{1-x_i\left(1+\frac{J_j}{J_i}\right)}{\mathcal{D}_{eff,ij}} + \frac{1}{D_{eff,Ki}} \right)$ is defined, so $u'(x_i) = \frac{1+\frac{J_j}{J_i}}{\mathcal{D}_{eff,ij}}$

$$\delta J_i = -C_t \int_{x_i=x_{i0}}^{x_{i\delta}} \frac{1}{u} \cdot \frac{\mathcal{D}_{eff,ij}}{1 + \frac{J_j}{J_i}}\,\partial u \tag{C.27}$$

$$= -\frac{C_t\,\mathcal{D}_{eff,ij}}{1 + \frac{J_j}{J_i}} \left[\ln(u)\right]_{u(x_{i\delta})}^{u(x_{i0})} \tag{C.28}$$

$$= -\frac{C_t\,\mathcal{D}_{eff,ij}}{1 + \frac{J_j}{J_i}} \ln \left(\frac{\frac{1-x_{i0}\left(1+\frac{J_j}{J_i}\right)}{\mathcal{D}_{eff,ij}} + \frac{1}{D_{eff,Ki}}}{\frac{1-x_{i\delta}\left(1+\frac{J_j}{J_i}\right)}{\mathcal{D}_{eff,ij}} + \frac{1}{D_{eff,Ki}}} \right) \tag{C.29}$$

$$\Leftrightarrow J_i = \frac{C_t\,\mathcal{D}_{eff,ij}}{\delta \cdot \left(1 + \frac{J_j}{J_i}\right)} \ln \left(\frac{1 - x_{i\delta}\left(1 + \frac{J_j}{J_i}\right) + \frac{\mathcal{D}_{eff,ij}}{D_{eff,Ki}}}{1 - x_{i0}\left(1 + \frac{J_j}{J_i}\right) + \frac{\mathcal{D}_{eff,ij}}{D_{eff,Ki}}} \right) \tag{C.30}$$

This result has been documented in the literature before[1], and is commonly used for calculations of Wicke-Kallenbach results. For $J_i = -J_j$, (C.26) reduce to:

$$\delta J_i = -C_t \int_{x_i=x_{i0}}^{x_{i\delta}} \left(\frac{1}{\mathcal{D}_{eff,ij}} + \frac{1}{D_{eff,K,i}} \right)^{-1} \partial x_i$$

$$= \frac{-C_t\,(x_{i\delta} - x_{i0})}{\frac{1}{\mathcal{D}_{eff,ij}} + \frac{1}{D_{eff,K,i}}}$$

$$\Leftrightarrow J_i = \frac{C_t \cdot (x_{i0} - x_{i\delta})}{\delta \cdot \left(\frac{1}{\mathcal{D}_{eff,ij}} + \frac{1}{D_{eff,K,i}} \right)} \tag{C.31}$$

$$\Leftrightarrow \frac{1}{\mathcal{D}_{eff,ij}} = \frac{C_t \cdot (x_{i0} - x_{i\delta})}{J_i\,\delta} - \frac{1}{D_{eff,K,i}}$$

[1](C.30) is identical to equation 3.5.2-14 in Froment and Bischoff (1990) and equation 4 in Haugaard and Livbjerg (1998)

$$\Leftrightarrow \mathcal{D}_{eff,ij} = \left(\frac{C_t \cdot (x_{i0} - x_{i\delta})}{J_i\, \delta} - \frac{1}{D_{eff,K,i}} \right)^{-1} \tag{C.32}$$

From (C.30) and (C.32) the effective diffusion coefficient was found from the diffusion velocity of species i, $v_i = J_i/C_t$ as:

$$\mathcal{D}_{eff,ij} = \begin{cases} \dfrac{\delta \cdot \left(1 + \frac{J_j}{J_i}\right)}{\ln\left(\frac{1 - x_{i\delta}\left(1 + \frac{J_j}{J_i}\right) + \frac{\mathcal{D}_{eff,ij}}{D_{eff,Ki}}}{1 - x_{i0}\left(1 + \frac{J_j}{J_i}\right) + \frac{\mathcal{D}_{eff,ij}}{D_{eff,Ki}}} \right)} v_i & \text{for } J_i \neq -J_j \\ \left(\frac{x_{i0} - x_{i\delta}}{v_i\, \delta} - \frac{1}{D_{eff,K,i}} \right)^{-1} & \text{for } J_i = -J_j \end{cases} \tag{C.33}$$

This conditional expression for $\mathcal{D}_{eff,ij}$ is continuous for all J_i and J_j. Grahams law gives the following relation for combined ordinary and Knudsen diffusion:

$$\begin{aligned} \frac{J_i}{J_j} &= -\sqrt{\frac{M_j}{M_i}} \\ \Leftrightarrow 1 + \frac{J_j}{J_i} &= 1 - \sqrt{\frac{M_i}{M_j}} \end{aligned} \tag{C.34}$$

so:

$$\mathcal{D}_{eff,ij} = \begin{cases} \dfrac{\delta \cdot \left(1 - \sqrt{\frac{M_i}{M_j}}\right)}{\ln\left(\frac{1 - x_{i\delta}\left(1 - \sqrt{\frac{M_i}{M_j}}\right) + \frac{\mathcal{D}_{eff,ij}}{D_{eff,Ki}}}{1 - x_{i0}\left(1 - \sqrt{\frac{M_i}{M_j}}\right) + \frac{\mathcal{D}_{eff,ij}}{D_{eff,Ki}}} \right)} v_i & \text{for } M_i \neq M_j \\ \left(\frac{x_{i0} - x_{i\delta}}{\delta\, v_i} - \frac{1}{D_{eff,K,i}} \right)^{-1} & \text{for } M_i = M_j \end{cases} \tag{C.35}$$

If Knudsen diffusion can be ignored ($D_{eff,K,i} \gg \mathcal{D}_{eff,ij}$), (C.35) is reduced to:

$$(\mathcal{D}_{eff,ij})_i = \begin{cases} \dfrac{\delta \cdot \left(1 - \sqrt{\frac{M_i}{M_j}}\right)}{\ln\left(\frac{1 - x_{i\delta}\left(1 - \sqrt{\frac{M_i}{M_j}}\right)}{1 - x_{i0}\left(1 - \sqrt{\frac{M_i}{M_j}}\right)} \right)} v_i & \text{for } M_i \neq -M_j \\ \dfrac{\delta}{x_{i0} - x_{i\delta}}\, v_i & \text{for } M_i = -M_j \end{cases} \tag{C.36}$$

where the index i in $(\mathcal{D}_{eff,ij})_i$ indicates that the value was estimated from the diffusive flux of gas i, J_i. A corresponding estimate $(\mathcal{D}_{eff,ij})_j$ based on J_j can be derived by

symmetry by swapping the gases i and j:

$$(\mathcal{D}_{eff,ij})_j = \begin{cases} \dfrac{\delta \cdot \left(1-\sqrt{\frac{M_j}{M_i}}\right)}{\ln\left(\frac{1-x_{j0}\left(1-\sqrt{\frac{M_j}{M_i}}\right)}{1-x_{j\delta}\left(1-\sqrt{\frac{M_j}{M_i}}\right)}\right)} v_j & \text{for } M_i \neq M_j \\ \\ \frac{\delta}{x_{j\delta}-x_{j0}} v_j & \text{for } M_i = M_j \end{cases} \tag{C.37}$$

The concentrations of the carrier gases at the outlet of the chambers are:

$$x_{j\delta} = 1 - x_{i\delta} \tag{C.38}$$
$$x_{i0} = 1 - x_{j0} \tag{C.39}$$

When it had not been possible to measure one of $x_{i\delta}$ or x_{j0}, Grahams law was used to estimate the missing concentration:

$$x_{i\delta} = \frac{F_i}{F_{\delta,in} + F_i} = \frac{\sqrt{\frac{M_j}{M_i}}\, F_j}{F_{\delta,in} + \sqrt{\frac{M_j}{M_i}}\, F_j} \tag{C.40}$$

or

$$x_{j0} = \frac{F_j}{F_{0,in} + F_j} = \frac{\sqrt{\frac{M_i}{M_j}}\, F_i}{F_{0,in} + \sqrt{\frac{M_i}{M_j}}\, F_i} \tag{C.41}$$

This estimate was only used for the calculation of $x_{j\delta}$ or x_{i0} in (C.38) or (C.39) in order to calculate the effective diffusion coefficient of the *measured* gas species.

C.2.1. Assuming pure Knudsen diffusion

If pure Knudsen diffusion can be assumed, (C.26) simplifies to:

$$\delta J_i = -C_t \int_{x_i=x_{i0}}^{x_{i\delta}} D_{eff,K,i}\, \partial x_i \tag{C.42}$$
$$= C_t \cdot (x_{i0} - x_{i\delta}) \cdot D_{eff,K,i} \tag{C.43}$$
$$\Leftrightarrow J_i = -C_t \frac{x_{i0} - x_{i\delta}}{\delta} \tag{C.44}$$
$$D_{eff,K,i} = \frac{\delta\, J_i}{(x_{i0} - x_{i\delta})\, C_t} = \frac{\delta}{x_{i0} - x_{i\delta}} v_i \tag{C.45}$$

This is exactly the same expression as the expression for $\mathcal{D}_{eff,ij}$ for $M_i = M_j$ in (C.36). Therefore, for $M_i = M_j$, it is a valid determination of the effective diffusion coefficient in either case, and since (C.36) is continuous, it is approximately so for $M_i \simeq M_j$. Inserting the expression for Knudsen diffusion (1.36):

$$D_{eff,K,i} = \frac{\phi}{\tau} \cdot \frac{4}{3} K_0 \sqrt{\frac{8\,R_u\,T}{\pi\,M_i}} = \frac{\delta}{x_{i0} - x_{i\delta}}\, v_i \tag{C.46}$$

$$\Leftrightarrow \frac{K_0\,\phi}{\tau} = \frac{3\,\delta}{(x_{i0} - x_{i\delta})} \sqrt{\frac{\pi\,M_i}{128\,R_u\,T}}\, v_i \tag{C.47}$$

The constant $\frac{K_0\,\phi}{\tau}$ is used to describe the porous medium, if pure Knudsen diffusion can be assumed. Formula (1.36) can be used to calculate the effective diffusion coefficient for a gas i at temperature T:

$$D_{eff,i} = D_{eff,i,K} = \frac{\phi}{\tau}\, D_{i,K} = \frac{4}{3} \left(\frac{K_0\,\phi}{\tau}\right) \sqrt{\frac{8\,R_u\,T}{\pi\,M_i}} \tag{C.48}$$

C.3. Finding Φ

For single gas flow with a pressure difference, $\nabla p \neq 0$, the Dusty Gas Model (1.57) reduce to:

$$-\nabla C = \frac{\vec{J_i}}{D_{eff,K,i}} + \frac{1}{D_{eff,K,i}} \left(\frac{p\,\vec{\Phi}}{R_u\,T\,\mu}\right) \nabla p \tag{C.49}$$

$$\begin{aligned} \Leftrightarrow \vec{J_i} &= -D_{eff,K,i}\,\nabla C - \left(\frac{p\,\vec{\Phi}}{R_u\,T\,\mu}\right) \nabla p \\ &= \frac{-D_{eff,K,i}}{R_u\,T}\,\nabla p - \left(\frac{p\,\vec{\Phi}}{R_u\,T\,\mu}\right) \nabla p \\ &= -\frac{1}{R_u\,T} \left(D_{eff,K,i} + \frac{p\,\vec{\Phi}}{\mu}\right) \nabla p \end{aligned} \tag{C.50}$$

again, for steady-state, isothermal one-dimensional flow without gas accumulation, the mole flux will be constant. The flux (along the z axis) though a porous material of thickness δ with pressures p_1 and p_2 at the ends can be derived:

$$\begin{aligned} \int_{\xi=0}^{\delta} J\,\partial\xi = J\,\delta &= \int_{\xi=0}^{\delta} \left(\frac{-D_{eff,K,i}}{R_u\,T} + \frac{C_t\,\Phi}{\mu}\right) \frac{\partial p}{\partial \xi}\,\partial\xi \\ &= \frac{-1}{R_u\,T} \int_{p=p_0}^{p_\delta} \left(D_{eff,K,i} + \frac{p\,\Phi}{\mu}\right) \partial p \end{aligned}$$

$$
\begin{aligned}
&= \frac{-1}{R_u\,T}\left(D_{eff,K,i}\cdot(p_\delta - p_0) + \frac{\Phi}{\mu}\int_{p=p_0}^{p_\delta} p\,\partial p\right) \\
&= \frac{-1}{R_u\,T}\left(D_{eff,K,i}\cdot(p_\delta - p_0) + \frac{\Phi}{2\,\mu}\left(p_\delta^2 - p_0^2\right)\right) \qquad \text{(C.51)} \\
\Leftrightarrow J &= \frac{-1}{R_u\,T\,\delta}\left(D_{eff,K,i}\cdot(p_\delta - p_0) + \frac{\Phi\,\left(p_\delta^2 - p_0^2\right)}{2\,\mu}\right) \\
&= \frac{p_0 - p_\delta}{R_u\,T\,\delta}\left(D_{eff,K,i} + \frac{\Phi\,\overline{p}}{\mu}\right) \qquad \text{(C.52)}
\end{aligned}
$$

where $\overline{p} = \frac{p_0+p_\delta}{2}$[2]. Here $D_{eff,K,i}$ is responsible for the well known phenomena *viscous slip*, where the viscous flow through a porous medium defers from the otherwise linear pressure dependence (Mason and Malinauskas, 1983).

Solving for the permeability, Φ:

$$\Phi = \frac{\mu}{\overline{p}}\left(J\,\frac{R_u\,T\,\delta}{p_0 - p_\delta} - D_{eff,K,i}\right) \qquad \text{(C.53)}$$

If the gas volume flow $\dot{\mathcal{V}}_\delta$ at pressure p_δ and the cross sectional area, A, are known, then:

$$\Phi = \frac{\mu}{\overline{p}}\left(\frac{p_\delta\,\delta}{p_0 - p_\delta}\cdot\frac{\dot{\mathcal{V}}_\delta}{A} - D_{eff,K,i}\right) \qquad \text{(C.54)}$$

The viscosities, μ, of the used gases are listed in Table 2.1 on page 88.

C.4. Uncertainty

In this appendix the uncertainty assessments for the Wicke-Kallenbach measurements is documented.

C.4.1. Sample geometry uncertainty

The precision of the Wicke-Kallenbach measurements depends on a number of parameters. The samples were oval shaped due to the orthotropic shrinkage. The major and minor diameters d_1 and d_2 as well as the sample length L were determined with a precision of ϵ_d=0.1 mm. If A^* is the determined area and A is the true area, the precision is:

$$\epsilon_A = |A - A^*| \qquad \text{(C.55)}$$

[2](C.52) correspond to equation 143 and 144 in Mason and Malinauskas (1983).

$$= |\pi\, d_1 d_2 - \pi\ (d_1 + \epsilon_d) \cdot (d_2 + \epsilon_d)| \quad \text{(C.56)}$$
$$= \pi\ \left((d_1 + d_2)\, \epsilon_d + \epsilon_d^2\right) \quad \text{(C.57)}$$

E.g. the smallest diameters were 12 and 15 mm. For ϵ_d =0.1 mm, the maximum uncertainty is 8.5 mm^2 or 1.5% of A^*. The uncertainty of L is ϵ_d, which is 1.1% of the smallest measured sample length.

C.4.2. Flow uncertainty

The flows were adjusted using mass flow controllers and determined with a soap bubble flowmeter. The flows could drift approximately 5 ml/min during the experiment. Even though the flow was measured as an average of 3 measurements shortly after the gas concentrations were deemed steady, the uncertainty of flow measurements are considered to be $\epsilon_F = 5$ ml/min. For flows exceeding 500 ml/min, 1% uncertainty was assumed.

For flows below 20 ml/min, a smaller NFC (50 ml/min) and flowmeter was used. The uncertainty for flows below 20 ml/min was approximately ϵ_F=0.1 ml/min.

C.4.3. Gas concentration uncertainty

Gas concentrations were detected with uncertainties ϵ_x of approximately ϵ_x=5 ppm for small concentrations. For concentrations exceeding 500 ppm, 3% uncertainty was assumed. Since all concentration determinations were a difference between the signal of the carrier gas and the actual signal, the maximum uncertainty was assumed twice these numbers.

C.4.4. Diffusive flow uncertainty

Since the diffusive flows are small compared to the carrier flows through the chambers (F_i, $F_j \ll F_{j,in}$, $F_{j,in}$), (2.1) reduce to:

$$F_i \simeq F_{j,in}\, x_{i\delta} \quad \text{(C.58)}$$

The uncertainty of the diffusive flow F_i, ϵ_{FDi} then become:

$$\epsilon_{FDi} = |F_i - F_i^*| \quad \text{(C.59)}$$
$$= |F_{j,in}\, x_{i\delta} - (F_{j,in} + \epsilon_{Fj})\ (x_{i\delta} + 2 \cdot \epsilon_{xi})| \quad \text{(C.60)}$$
$$= 2\, \epsilon_{xi}\ (F_{j,in} + \epsilon_{Fj}) + x_{i\delta}\, \epsilon_{Fj} \quad \text{(C.61)}$$

For a carrier gas flow of $F_{i,in} = F_{j,in} = 0.500\,\mathrm{l/min}$ and gas concentration $x_{i\delta} = 60\,\mathrm{ppm}$, the uncertainty will be:

$$\epsilon_{FDi} = 2 \cdot 10 \cdot 10^{-6} \cdot \left(0.5 \frac{\mathrm{l}}{\mathrm{min}} + 0.005 \frac{\mathrm{l}}{\mathrm{min}}\right) + 60 \cdot 10^{-6} \cdot 0.005 \frac{\mathrm{l}}{\mathrm{min}}$$

$$= 1.04 \cdot 10^{-6} \frac{\mathrm{l}}{\mathrm{min}}$$

which is a relative uncertainty of 3.0%.

C.4.5. Diffusion coefficient uncertainty

The diffusive flux is calculated as $v_i = F_i/A$. The maximum uncertainty will be:

$$|v_i - v_i^*| = \frac{F_i}{A} - \frac{F_i + \epsilon_{FDi}}{A - \epsilon_A} \tag{C.62}$$

E.g. for a carrier flow of $F_{i,in} = F_{j,in}$=0.500 l/min, a measured concentration of 60 ppm and minor and major sample diameter of d_1=12 mm and d_2=15 mm, it is:

$$F_i \simeq 0.5 \cdot 60 \cdot 10^{-6} = 30 \cdot 10^{-6}\,\mathrm{l/min} \tag{C.63}$$

$$v_i \simeq \frac{30 \cdot 10^{-6}\,\mathrm{l/min}}{565.5\,\mathrm{mm}^2} = 884 \cdot 10^{-9}\,\mathrm{m/s} \tag{C.64}$$

$$\epsilon_{vi} = \frac{30 \cdot 10^{-6}\,\mathrm{l/min}}{565.5\,\mathrm{mm}^2} - \frac{30 \cdot 10^{-6}\,\mathrm{l/min} + 0.91 \cdot 10^{-6}\,\mathrm{l/min}}{565.5 - 8.45\,\mathrm{mm}^2} \tag{C.65}$$

$$= 40.5 \cdot 10^{-9}\,\mathrm{m/s} \tag{C.66}$$

which is a 4.6% relative uncertainty.

In order to find the uncertainty of the determination of $\mathcal{D}_{eff,ij}$ (C.36), the simple form (for $M_i = M_j$) will be assumed, and $x_{i0} - x_{i\delta}$ will be assumed close to unity:

$$\mathcal{D}_{eff,ij} = \frac{\delta}{(x_{i0} - x_{i\delta})} v_i \tag{C.67}$$

$$\simeq \delta \cdot v_i \tag{C.68}$$

$$\epsilon_{\mathcal{D}eff,i} = \left|\mathcal{D}_{eff,ij} - \mathcal{D}^*_{eff,ij}\right| \tag{C.69}$$

$$= |L \cdot v_i - (L + \epsilon_d) \cdot (v_i + \epsilon_{vi})| \tag{C.70}$$

$$= \epsilon_{vi}\,(L + \epsilon_d) + v_i \cdot \epsilon_d \tag{C.71}$$

In our example, this yields:

$$\mathcal{D}_{eff,ij} = \frac{0.009\,\mathrm{m}}{1}\, 884 \cdot 10^{-9}\,\mathrm{m/s} = 7.96 \cdot 10^{-9}\,\mathrm{m}^2/\mathrm{s}$$

$$\epsilon_{\mathcal{D}eff,i} = 40.5 \cdot 10^{-9}\,(0.009\,\mathrm{m} + 0.0001\,\mathrm{m}) + 884 \cdot 10^{-9}\,\mathrm{m/s} \cdot 0.0001\,\mathrm{m}$$

$$= 0.457 \cdot 10^{-9}\,\mathrm{m^2/s}$$

a relative uncertainty of 5.7%.

Figure C.1 shows the diffusion coefficient ratio plot from Figure 3.14 on page 125 with added error bars. The uncertainties were within 17–21% except for the 0% converted R and T samples, where the low diffusive flux increased the uncertainty up to 40%.

C.4.6. Permeability uncertainty

The uncertainty is determined as the difference between the true value and the highest possible permeability value due to measurement uncertainties:

$$\begin{aligned} \epsilon_{\mathcal{D}eff,i} &= \left|\mathcal{D}_{eff,ij} - \mathcal{D}^*_{eff,ij}\right| \\ &= \frac{(L+\epsilon_d)\cdot\left(1-\sqrt{\frac{M_i}{M_j}}\right)}{\ln\left(\frac{1-\left(x_{i,L}+\epsilon_d\right)\left(1-\sqrt{\frac{M_i}{M_j}}\right)}{1-\left(x_{i,0}-\epsilon_d\right)\left(1-\sqrt{\frac{M_i}{M_j}}\right)}\right)}\,(v_i+\epsilon_{vi}) - \mathcal{D}_{eff,ij} \end{aligned} \tag{C.72}$$

The uncertainty of the permeability determination (C.54) from measurement uncertainties is calculated the same way:

$$\epsilon_\Phi = \frac{-2\mu}{p_1+p_2-\epsilon_{dp}}\left(\frac{p_2\,(L+\epsilon_d)}{p_2-p_1+\epsilon_{dp}}\cdot(v_d+\epsilon_v)\right) - \Phi \tag{C.73}$$

where ϵ_{dp} is the uncertainty of the pressure difference measurement. It was 0.5 Pa for pressure differences below 20.000 Pa and 2.000 for higher pressure differences. ϵ_v is the uncertainty of the normal gas velocity of gas through the sample, v:

$$\epsilon_v = \frac{F_{out}+\epsilon_F}{A-\epsilon_A} - \frac{F_{out}}{A} \tag{C.74}$$

where F_{out} is the measured normal gas flow out of the setup, and ϵ_F is the absolute uncertainty of this value.

Figure C.2 shows the permeability results with added error bars. In Figure C.2a, the uncertainties where assessed as described above. The uncertainties were 8–10% except for R and T samples with a high degree of conversion, where uncertainty reached 15%. In Figure C.2b, the error bars shows the standard deviation of repeated measurements.

C.4.7. Combined uncertainty of several measurements

Each measurement i resulted in a value, y_i and a corresponding uncertainty, ϵ_i, calculated as shown above. It was interpreted as a stochastic variable with the normal distribution

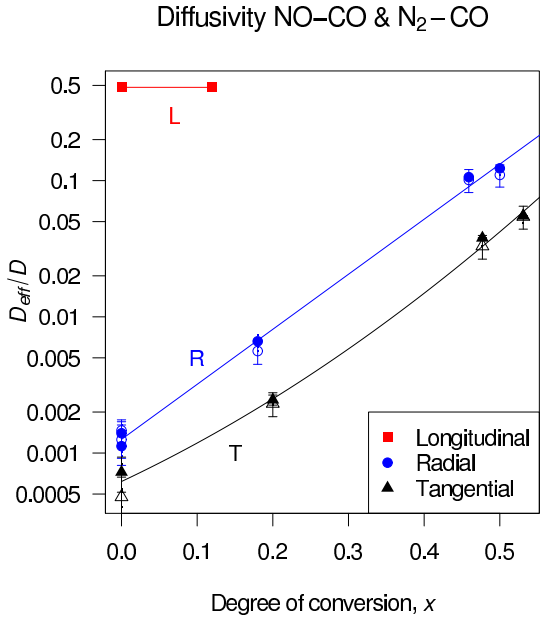

(a) Diffusion results with gas pairs NO-CO and N_2-CO. □ ○ △: NO; ■ ● ▲: CO.

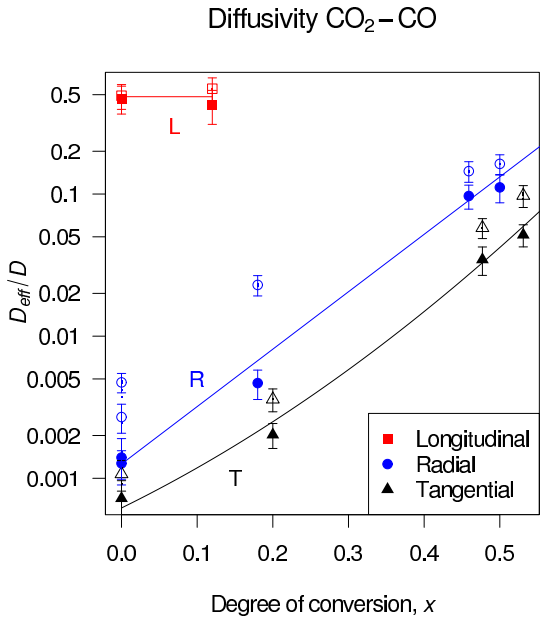

(b) Gas pair CO_2-CO. □ ○ △: CO_2; ■ ● ▲: CO.

Figure C.1.: Measurement uncertainties for measured diffusion coefficients. (Same as Figure 3.14 on page 125 with added error bars).

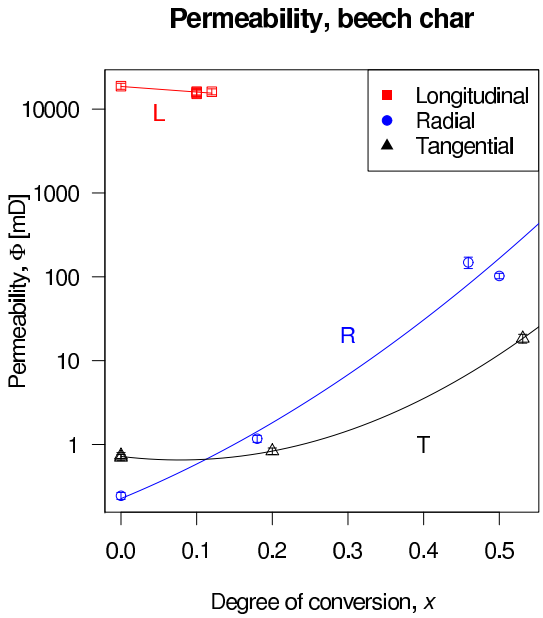

(a) Measurement uncertainty error bars.

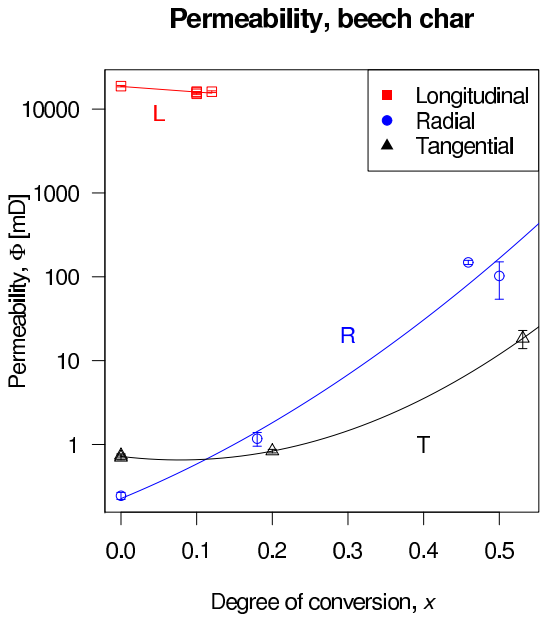

(b) Sample standard deviance error bars.

Figure C.2.: Uncertainties of permeability measurements. a: assessed measurement uncertainty b: Measurement standard deviation. (Same as Figure 3.16 on page 127 with added error bars).

$N(y_i, \epsilon_i^2)$[3] describing the probability of where to find the true value. The mean value, y_m, of the combined normal distributions of several measurements of the same property was then calculated as the maximum likelihood estimate. The propability density function for a normal distribution is:

$$f(y) = \frac{1}{\epsilon \cdot \sqrt{2\pi}} e^{-\frac{1}{2}\left(\frac{x-y}{\epsilon}\right)^2}$$

where y is the mean value and ϵ is the standard deviation. The propability of the true value being x, given n measurements, represented by the normal distributed stochastic variables $Y_1, Y_2 \ldots Y_n$, is:

$$\begin{aligned}
p\left(X = x | Y_!, Y_2 \ldots Y_n\right) &= p\left(Y_1 = x\right) \cap p\left(Y_2 = x\right) \cap \ldots \cap p\left(Y_n = x\right) && \text{(C.75)}\\
&= p\left(Y_1 = x\right) \cdot p\left(Y_2 = x\right) \cdot \ldots \cdot p\left(Y_n = x\right) && \text{(C.76)}\\
\Leftrightarrow f\left(X = x | Y_!, Y_2 \ldots Y_n\right) &= f\left(Y_1 = x\right) \cdot f\left(Y_2 = x\right) \cdot \ldots \cdot f\left(Y_n = x\right) && \text{(C.77)}\\
&= \frac{1}{\epsilon_1 \cdot \sqrt{2\pi}} e^{-\frac{1}{2}\left(\frac{x-y_1}{\epsilon_1}\right)^2} \cdot \frac{1}{\epsilon_2 \cdot \sqrt{2\pi}} e^{-\frac{1}{2}\left(\frac{x-y_2}{\epsilon_2}\right)^2} && \text{(C.78)}\\
&\quad \cdot \ldots \cdot \frac{1}{\epsilon_n \cdot \sqrt{2\pi}} e^{-\frac{1}{2}\left(\frac{x-y_n}{\epsilon_n}\right)^2} && \text{(C.79)}\\
&= \frac{1}{\left(\Pi_{i=1}^{n} \epsilon_i\right) \cdot (2\pi)^{n/2}} e^{-\frac{1}{2} \cdot \left(\sum_{i=1}^{n}\left(\frac{x-y_i}{\epsilon_i}\right)^2\right)} && \text{(C.80)}
\end{aligned}$$

The maximum likelihood estimate, $\hat{x}$, of the measured property is found as the value of x, which maximises $f\left(X = x | Y_!, Y_2 \ldots Y_n\right)$:

$$\begin{aligned}
\max_x \left(f\left(X = x | Y_!, Y_2 \ldots Y_n\right)\right) &= \max_x \left(e^{-\frac{1}{2} \cdot \left(\sum_{i=1}^{n}\left(\frac{x-y_i}{\epsilon_i}\right)^2\right)}\right) && \text{(C.81)}\\
&= \min_x \left(\sum_{i=1}^{n}\left(\frac{x-y_i}{\epsilon_i}\right)^2\right) && \text{(C.82)}\\
&= \min_x \left(x^2 \cdot \left(\sum_{i=1}^{n}\frac{1}{\epsilon_i^2}\right) - 2\,x \cdot \left(\sum_{i=1}^{n}\frac{y_i}{\epsilon_i^2}\right)\right. && \text{(C.83)}\\
&\quad \left. + \left(\sum_{i=1}^{n}\left(\frac{y_i}{\epsilon_i}\right)^2\right)\right) && \text{(C.84)}
\end{aligned}$$

The last sum is independant of x, and can be ignored, so:

$$\max_x \left(f\left(X = x | Y_!, Y_2 \ldots Y_n\right)\right) = \min_x \left(x^2 \cdot \left(\sum_{i=1}^{n}\frac{1}{\epsilon_i^2}\right) - 2\,x \cdot \left(\sum_{i=1}^{n}\frac{y_i}{\epsilon_i^2}\right)\right) \quad \text{(C.85)}$$

[3]Normal distribution having mean value y_i and standard deviation ϵ_i.

$$= \min_x \left(x^2 - 2x \cdot \frac{\sum_{i=1}^n \frac{y_i}{\epsilon_i^2}}{\sum_{i=1}^n \frac{1}{\epsilon_i^2}} \right) \tag{C.86}$$

$$= \min_x \left(\left(x - \frac{\sum_{i=1}^n \frac{y_i}{\epsilon_i^2}}{\sum_{i=1}^n \frac{1}{\epsilon_i^2}} \right)^2 \right) \tag{C.87}$$

Thus, the maximum likelihood estimate of the measured property, given all n measurements, is:

$$\hat{x} = \frac{\sum_{i=1}^n \frac{y_i}{\epsilon_i^2}}{\sum_{i=1}^n \frac{1}{\epsilon_i^2}} \tag{C.88}$$

Bayesian calculations give the same result as well as the following expression for the uncertainty of $\hat{x}$, $\epsilon_{\hat{x}}$, assuming that the measured values, y_i, are not very different (Box and Tiao, 1992):

$$\epsilon_{\hat{x}} = \sqrt{\frac{1}{\sum_{i=1}^n \left(\frac{1}{\epsilon_i^2} \right)}} \tag{C.89}$$

Since the results of each meaurement in some cases *did* differ significantly (especially properties in the R and T directions at 0% conversion), the uncertainty of $\hat{x}$ was instead conservatively assumed equal to the minimal measurement uncertainty covered:

$$\epsilon_{\hat{x}} = \min(\epsilon_i) \tag{C.90}$$

C.5. CO_2 deviations

As mentioned in Section 3.5.4 on page 138, diffusion measurements where the gas CO_2 was involved, resulted in violation of Grahams law, as the flux of CO_2 was higher than would be expected from the counter-diffusion species and measurements with other gas pairs. Figure C.3 on the next page shows the relative deviations from Grahams law for the individual measurements for the gas pair NO-CO (C.3a) and CO-CO_2 (C.3b) grouped by sample. Except for sample T5, the NO-CO measurements agreed with Grahams law within 14%. Sample T5 was the sample with least diffusive flux measured, and thus the highest uncertainty ($\pm$40% for $\frac{D_{eff}}{\mathcal{D}}$), which can explain the large deviation for this particular sample. In appendix C.72 the uncertainty of $\frac{D_{eff}}{\mathcal{D}}$ for the other samples were assessed to 17–21%, mainly influenced by the uncertainty of the determination of the diffusive flows. Therefore the deviations for NO-CO were within the level of uncertainty. On the contrary, CO-CO_2 measurements deviated by approximately 50% for most of the measurements, and up to 200–400% for samples with low diffusive fluxes. These deviations were clearly systematic, since all but one of the CO-CO_2 deviations were caused by excess diffusive flow of CO_2 (positive deviations in Figure C.3b).

This appendix documents the investigations made in order to identify the reason for this behaviour.

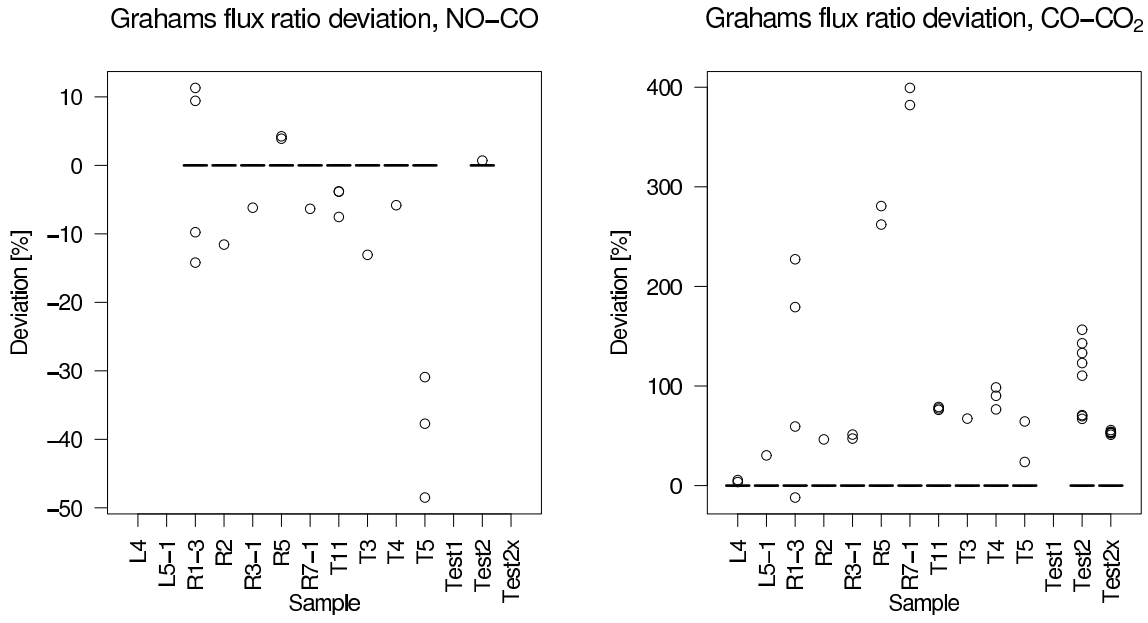

(a) NO-CO gas pair

(b) CO-CO_2 gas pair

Figure C.3.: Grahams law deviations, NO-CO and CO-CO_2 gas pairs.

C.5.1. Mass of gas in pipes

Initially, the setup was mounted in vertical orientation, so that the exit pipes from the W-K cell pointed upwards. It turned out that a significant pressure difference developed due to the difference in masses of the gas in the two exit pipes. The pressure difference had not been considered in the design phase, but corresponded well to the theoretical pressure difference caused by the masses of the gas in the exit pipes, Δp, which can be found this way:

$$\begin{aligned} \rho &= \frac{n\,M}{V} = \frac{M\,p}{R_u\,T} \\ p &= \rho\,g\,h = \frac{M\,p\,g\,h}{R_u\,T} \\ \Delta p &= \frac{(M_1 - M_2)\cdot p\,g\,h}{R_u\,T} \end{aligned}$$

where ρ is the density of the gas, p is the gauge pressure in the cell caused by the gas column, h is the height of the gas column ($h = 0.65$ m in the setup), and M_1 and M_2 are the molar masses of the two gases. For the gas pair CO-CO_2 at 295 K, Δp became 4.2 Pa, which was identical to the measured pressure difference using these gases. Therefore the setup was turned so that the exit pipes were horizontal, and this eliminated the measured

pressure difference. All of the reported measurements (including Figure C.3) were made in this position.

C.5.2. Gas analysis linearity?

A source of error could be the cross sensitivity of the gas analysis to the carrier gas. For each gas pair, the cross sensitivities were accounted for by measuring the gas analyser signals when fed directly from the other gas feed. This signal (less than 42 ppm) would then be subtracted from the values measured during the experiments. Measurements of the CO_2 analyser in a binary mixture of CO-CO_2 mixed from the gas flasks used during the W-K experiments (corrected for the signal from 100% CO) , and N_2-CO_2 are shown in Figure C.4. The analyser had been calibrated with a test gas consisting of 1001 ppm CO_2 and 1001 ppm CO. The excellent agreement between CO_2 measurements in CO ($\circ$) and N_2 ($\triangle$) confirmed that the linearity and sensitivity of the CO_2 gas analyser was unaffected by the presence of CO.

C.5.3. Surface diffusion?

Prior investigators have attributed similar differences for CO_2 diffusion in carbons to high surface areas and microporosity to surface diffusion (Wicke and Kallenbach, 1941; Mugge, 2000), supported by the fact that CO_2 diffusion increased more than expected with increasing pressure and decreased temperature. The Wicke Kallenbach cell in this work was not designed for variations in temperature. Even though the setup was designed to work with pressures up to 5 bar gauge, this was avoided due to the toxicity of the gases. Instead, diffusion measurements were made on a test species with low surface area and no microporosity: the acrylic test species with 59 drilled holes with radii of approximately 0.2 mm, labeled "Test 2". It was assumed that no significant surface diffusion could occur in this sample. The resulting diffusion coefficient ratios for several different gas pairs are shown in Figure C.5. The x-axis indicate variations in the inlet flows to the W-K cell, which will be used in the next section. $\frac{D_{eff}}{\mathcal{D}}$ for CO_2 and CO was 0.012 and 0.006 for CO_2-CO tests (symbols C and c in Figure C.5). NO-CO tests resulted in consistent values of $\frac{D_{eff}}{\mathcal{D}}$ for NO and CO of 0.0084 (symbols F and f), and in good agreement with the measurement of CO in N_2 (symbol e). These results complemented the measurements on char samples; measurements with NO-CO satisfied Grahams law, while CO_2 flux was larger than expected. While this did not rule out the presence of surface diffusion during measurements on char, it did indicate that some other unknown effect influenced the measurements with CO_2.

C.5.4. Insufficient mixing?

Another reason for the CO_2 effect could be insufficient mixing of gases in the W-K chambers. This could cause concentrations gradients in the exit pipes and lead to non-representative concentration measurements. One indication of insufficient mixing could

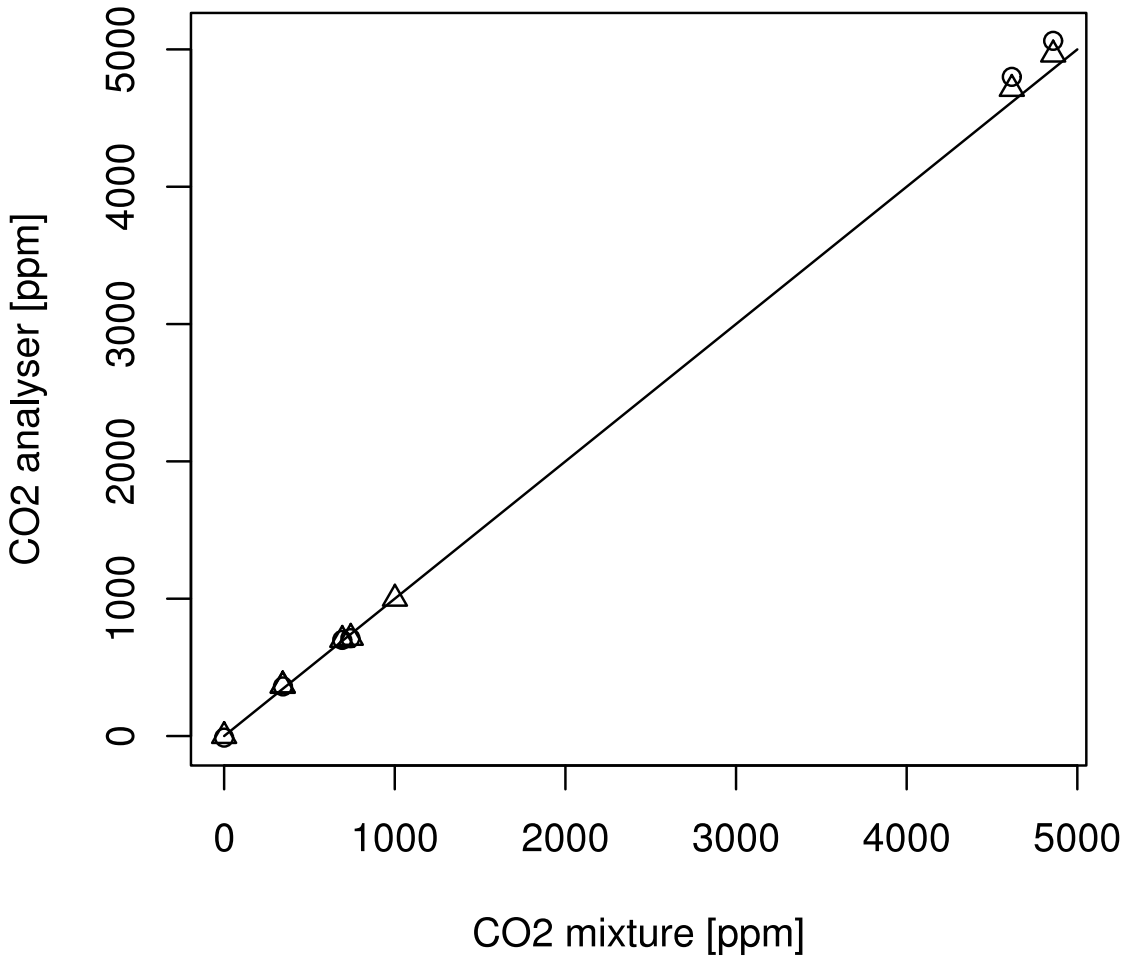

Figure C.4.: Linearity of CO_2-analyzer in carrier gases N_2 ($\triangle$) and CO ($\circ$). The analyzer had been calibrated with test gas with 1001 ppm CO_2 and 1001 ppm CO in N_2.

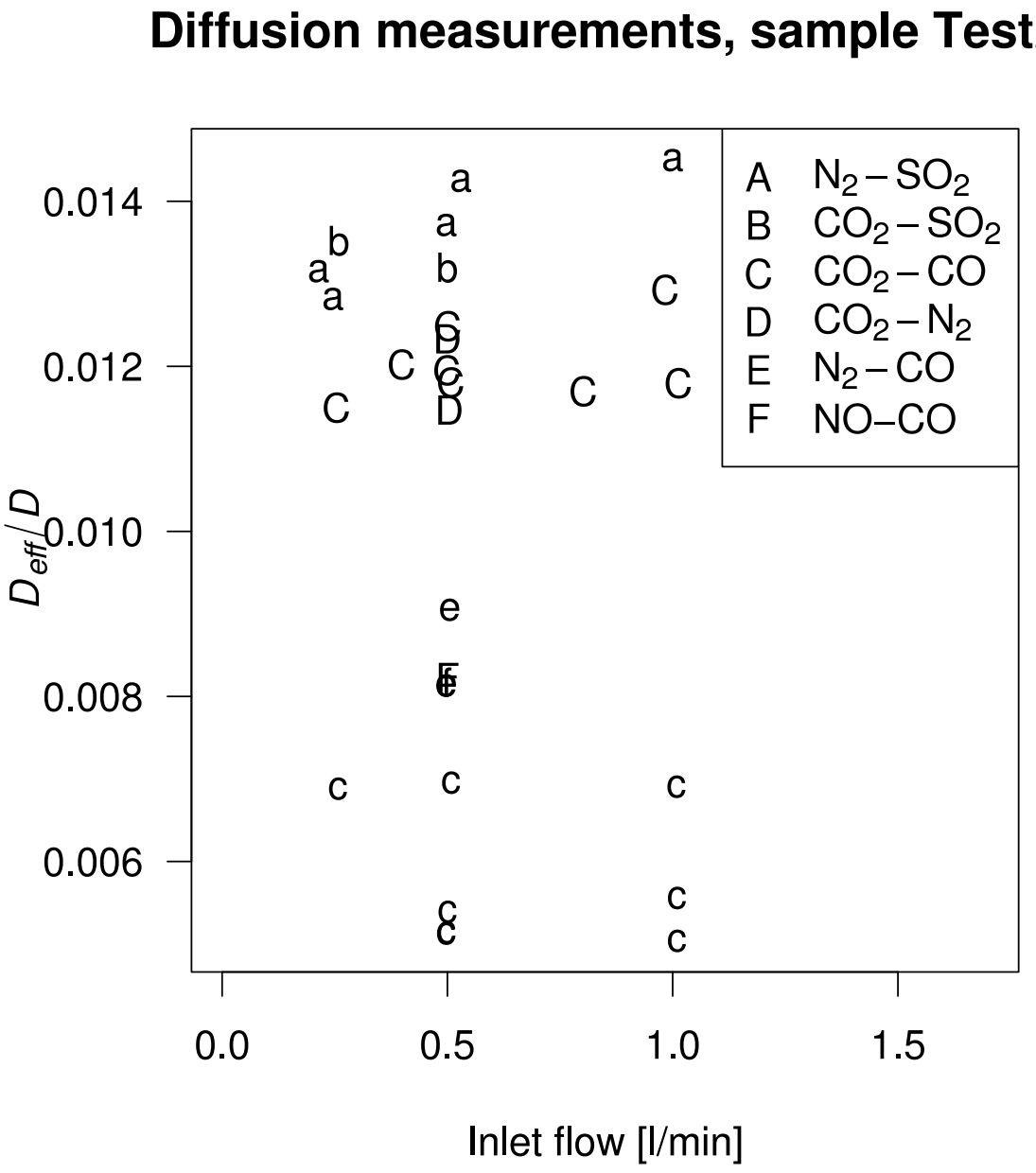

Figure C.5.: Diffusion measurements with different gas pairs on the Test2 reference sample. Upper and lower case letters mark measurements with first and second gas in the gas pair. (E.g. an upper case "C" is for CO_2 in counter flow with CO, while "c" is CO in counter flow with CO_2.)

be fluctuations in the measured concentrations caused by turbulence. Such fluctuations were not observed (see Figure 3.12 on page 122).

Applying different gas flows into the W-K cells would change the flow pattern in the cell and pipes, increasing the level of turbulence and mixing with higher flows. Even though such variations changed the absolute gas concentrations, Figure C.5 shows that they did not have any significant effect on the measured diffusion coefficient ratios.

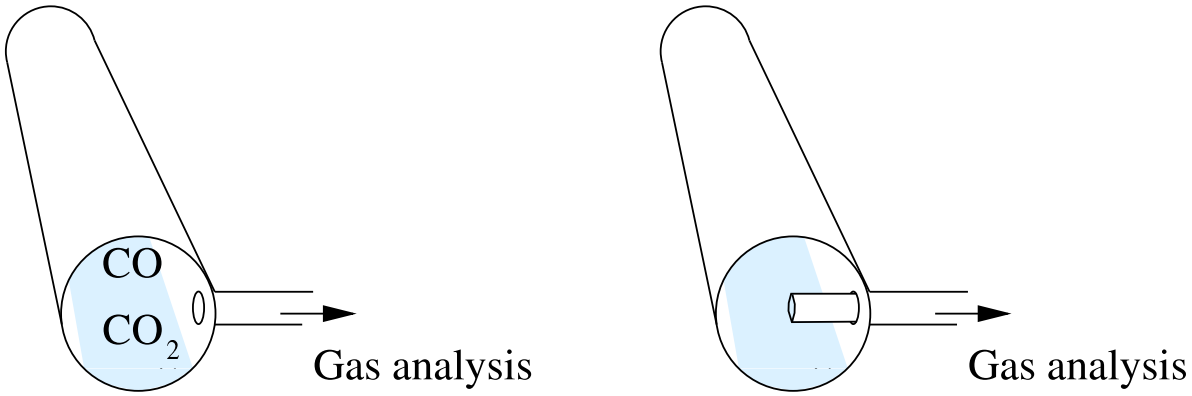

(a) Layout of gas analysis sample point in U-tube

(b) Inset to sample the gas in the middle of the U-tube

Figure C.6.: Gas analyser sample point. Standard layout (a), and modified to sample gas in the middle of the U-tube (b).

Figure C.6a shows the design of the sample gas analysis sample points in the exit pipes. The gas sample was drawn from a hole in the pipe wall. A simple modification causing the the gas to be drawn from the center of the pipe (Figure C.6) did not change the measured concentrations during measurements with CO-CO_2. This confirmed that there was no concentration difference between the default sample point and the center of the pipe.

No indications of insufficient mixing were found.

C.5.5. Another heavy gas?

One relevant property, where CO_2 differed significantly from the other gases used, was its molar mass, M=44 g/mol, where the other gases used had molar masses of 28 and 30 g/mol. The last attempt to identify the cause of the deviations were to introduce another heavy gas. SO_2 (M=64 g/mol) was chosen due the availability of a pure gas source and a suitable SO_2 gas analyser. Measurements on the Test2 sample with the gas pairs CO_2-SO_2 and N_2-SO_2 were included in Figure C.5. Only the SO_2 fluxes could be measured due to very strong cross sensitivity with SO_2 on the CO_2 analyser, so Grahams law could not be evaluated by simultaneous measurement of the counter diffusing species. But it was clear that the measured $\frac{D_{eff}}{D}$ for SO_2 was consistently higher than for any of the other gases, indicating a higher than expected diffusive SO_2 flow, just as was the case for CO_2.

Thus, SO_2 seems to show deviations similar to that of CO_2. The cause of the deviations may somehow be related to the higher molar masses (and gas densities) of these two gases. Other similarities between the two gases exist. E.g. both have high values of Lennard-Jones energies, $\frac{\epsilon}{\kappa}$, which may increase their tendency to adsorb to surfaces. Since the SO_2 measurements were made on a sample with low surface area, this was not expected to be important in these cases.

C.5.6. Rejection of CO_2 measurements

To conclude, the reason for the deviations for diffusion measurements including CO_2 gas was not identified. Therefore, the diffusion measurements made with this gas was not used to characterize the diffusion coefficients of the char samples.

D. HSM temperature estimation

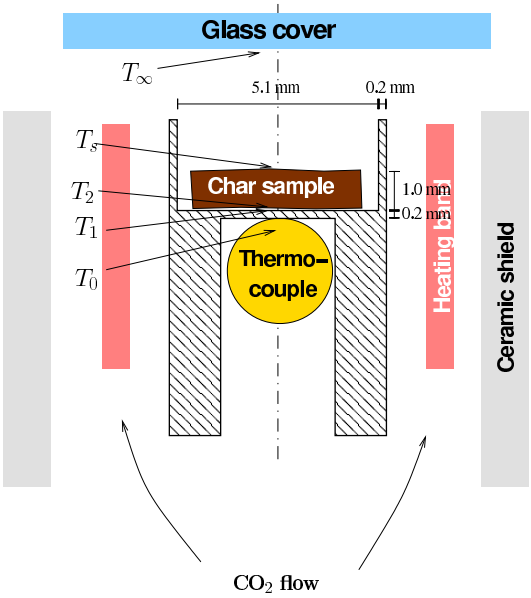

Figure D.1.: HSM crucible with temperature points used for calculations (See photo in Figure 2.8).

Figure D.1 shows a drawing of the heating stage oven with a char sample in the crucible. In order to calculate an upper limit for the expected difference between the sample surface temperature, T_s, and the thermocouple temperature, T_0, one-dimensional vertical heat flux from the thermocouple through the steel and char was assumed. The lower surface of the steel vial below the sample was assumed to have the temperature measured by the thermocouple, T_0. A 0.2 mm thick steel layer and 1.0 mm char layer separated the thermocouple from the observed char surface. The steel and char was in contact, but due to irregularities in the char geometry, this contact is not perfect. In order to make a very conservative estimate, it was assumed that there was *no direct contact*, and that a gap filled with CO_2 gas existed between the char and the steel. The char surface was assumed a perfect black body. It radiated heat to the surroundings, which were very conservatively assumed a perfect black body with the temperature 20 °C. The following data were used:

- Thermal conductivity of steel: 23.2 W/m·K (AISI 316 at 660 °C)
- Thermal conductivity of CO_2 between steel and char: 41.6 mW/m·K (CO_2 at 327 °C)

- Thermal conductivity of char: 2.47 W/m·K ("amorphous carbon" at 660 °C)
- Gap between steel and char: 50 μm (no direct contact)
- Emissivity of steel: 0.4

The heat fluxes through the layers, from the thermocouple to the observation glass:

- Steel: $\frac{q}{A} = \frac{k}{L}\,\Delta T = \frac{23.2\,\mathrm{W/m{\cdot}K}}{0.2{\cdot}10^{-3}\,\mathrm{m}} \cdot (T_0 - T_1) = 116 \cdot (T_0 - T_1)\ \mathrm{W/m^2}$
- Steel-char radiation: $\frac{q}{A} = 0.4\,\sigma_B\ (T_1^4 - T_2^4)$
- Steel-char conduction: $\frac{q}{A} = \frac{k}{L}\,\Delta T = \frac{41.6\,\mathrm{mW/m{\cdot}K}}{5{\cdot}10^{-5}\,\mathrm{m}} \cdot (T_0 - T_1) = 832 \cdot (T_1 - T_2)\ \mathrm{W/m^2}$
- Char: $\frac{q}{A} = \frac{2.47\,\mathrm{W/m{\cdot}K}}{1.0{\cdot}10^{-3}\,\mathrm{m}} \cdot (T_2 - T_s) = 2.47 \cdot (T_2 - T_s)\ \mathrm{W/m^2}$
- Surface radiation: $\frac{q}{A} = \sigma_B\ (T_s^4 - T_\infty^4)$

where (see Figure 2.8) T_0 is the thermocouple temperature, T_1 is the temperature at the upper steel surface, T_2 is the temperature at the lower char surface, T_s is the sample surface temperature, T_∞ is the temperature of the surroundings and $\sigma_B = 5.67 \cdot 10^{-8}\,\mathrm{W/\left(m^2\,K^4\right)}$ is the Stefan-Boltzmann constant.

Choosing T_0=973 K (700 °C) and T_∞=293 K and solving for T_1, T_2 and T_s, the results were: T_1=699.7 °C, T_2=657 °C and T_s=641 °C. In the gap, 10% of the heat flux occurred as radiation, while 90% was heat conduction through the CO_2. The sample surface in this very conservative estimate would differ from the thermocouple temperature by roughly 60 °C.

Two of the assumptions were expected to cause a significant overestimation of the temperature difference: The majority of the temperature drop occurs in the gas between the steel and char, where direct solid contact was not included in the calculation, even though there must be physical contact at at least three points, as the sample rests on the steel surface. The temperature of the surroundings, T_∞, was assumed room temperature, even through the glass surface inside the oven must have a significantly higher temperature. In addition, the heat conductivity of CO_2 was taken at 327 °C, which is much lower than the actual temperature range. Both lead to a significant under estimation of the heat flux in the gap, an thus an over estimation of the temperature difference, so the temperature difference must be expected to be significantly lower than the estimated 60 °C. In addition, the calculation is very sensitive to the actual width of the gap. A new calculation, where the gap was ignored ($T_1 = T_2$), the temperature difference was between T_0 and T_s was 19 °C. So the *conservative* estimates of the temperature difference between sample surface and thermocouple was assumed somewhere between 19 and 60 °C.

E. Slab model

This appendix describe how the model calculations of the slab gasification model described in Section 4 on page 155, were performed.

E.1. Mathematical description

In this section, the actual calculations performed by the program are presented. The stiff backward differentiation version of the lsode solver in the Matlab clone Octave[1] was used. It solves coupled ordinary differential equations (ODE) of the standard form:

$$\frac{\partial \vec{Y}}{\partial t} = f(\vec{Y}, t) \tag{E.1}$$

$$\vec{Y}_{t=0} = \vec{Y}_0 \tag{E.2}$$

The following values for each node are stored in the model:

- Char density ρ_{char} (mass of char per volume *including* porosity) [kg/m^3]
- Gas concentrations $C_{\mathrm{N_2}}$, $C_{\mathrm{H_2}}$, C_{CO}, $C_{\mathrm{H_2O}}$ and $C_{\mathrm{CO_2}}$ (mol gas per *void volume*) [mol/m^3]

The initial values $\vec{Y}_{t=0}$ were initialised according to the initial values given above.

E.1.1. Intermediate variables

The following temporary variables were calculated in the user defined solver routine `f_resid()` during each iteration before the actual derivatives for (E.1) were given. The reactivities $R_{\mathrm{CO_2}}$, $R_{\mathrm{H_2O}}$ and R_{WGS} in each node were found using (4.17)–(4.20). The degree of conversion was calculated from the initial char density, $\rho_{char,0}$:

$$X_n = 1 - \frac{\rho_{char,n}}{\rho_{char,0}} \tag{E.3}$$

The local porosity:

$$\phi_n(X_n) = 0.7 + 0.3\,X_n \tag{E.4}$$

[1] Open source software package at http://www.octave.org

Gas productions:

$$\begin{pmatrix} \dot{\Gamma}_{\mathrm{H_2O}} \\ \dot{\Gamma}_{\mathrm{H_2}} \\ \dot{\Gamma}_{\mathrm{CO}} \\ \dot{\Gamma}_{\mathrm{CO_2}} \end{pmatrix} = \left(\begin{pmatrix} -1 \\ +1 \\ +1 \\ 0 \end{pmatrix} \cdot R_{\mathrm{H_2O}} + \begin{pmatrix} 0 \\ 0 \\ +2 \\ -1 \end{pmatrix} \cdot R_{\mathrm{CO_2}} \right) \cdot \frac{\rho_{char}}{12\,\mathrm{g/mol}} + \begin{pmatrix} -1 \\ +1 \\ -1 \\ +1 \end{pmatrix} \cdot R_{WGS} \quad \text{(E.5)}$$

Discrete partial length derivatives of properties (C_i, T) for node n were found using the finite differences (for property α) for nodes $n \in [1 : N+1]$:

$$\frac{d\alpha_{i,n}}{d\xi} = \frac{\alpha_{i,n+1} - \alpha_{i,n-1}}{2\,d\xi} \quad \text{(E.6)}$$

$$\frac{d^2\alpha_{i,n}}{d\xi^2} = \frac{\alpha_{i,n+1} + \alpha_{i,n-1} - 2\,\alpha_{i,n}}{(d\xi)^2} \quad \text{(E.7)}$$

$\alpha_{i,0}$ existed to hold the constant values for the boundary temperature and gas concentrations. The derivatives for the last node, N, was defined to enforce the boundary condition of zero first derivatives in temperature and concentrations. The second derivatives were determined by considering the virtual node number $N+1$ mirroring the properties of node $N-1$, so that $\alpha_{N+1} = \alpha_{N-1}$:

$$\frac{d\alpha_{i,N}}{d\xi} = 0 \quad \text{(E.8)}$$

$$\frac{d^2\alpha_{i,N}}{d\xi^2} = \frac{\alpha_{i,N+1} + \alpha_{i,N-1} - 2\,\alpha_{i,N}}{(d\xi)^2} \quad \text{(E.9)}$$

$$= \frac{2\alpha_{i,N-1} - 2\alpha_{i,N}}{(d\xi)^2} \quad \text{(E.10)}$$

The local total gas concentrations, $C_{t,n}$ and pressures, p_n, were found using the ideal gas law:

$$C_{t,n} = \sum C_{i,n} \quad \text{(E.11)}$$

$$p_n = R_u T_n\, C_{t,n} \quad \text{(E.12)}$$

The following partial derivatives for the total gas concentrations, $C_{t,n}$ and pressures, p_n, mole fractions, x_i and gas fluxes were then calculated:

$$\frac{dC_{t.n}}{d\xi} = \sum \frac{dC_{i.n}}{d\xi} \quad \text{(E.13)}$$

$$\frac{d^2C_{t.n}}{d\xi^2} = \sum \frac{d^2C_{i.n}}{d\xi^2} \quad \text{(E.14)}$$

$$\frac{dp}{d\xi} = R_u \left(\frac{dT_n}{d\xi} \cdot C_{t,n} + T_n \cdot \frac{dC_{t,n}}{d\xi} \right) \tag{E.15}$$

$$\frac{d^2p_n}{d\xi^2} = R_u \left(\frac{d^2T_n}{d^2\xi} \cdot C_{t,n} + 2\,\frac{dT_n}{d\xi} \cdot \frac{dC_{t,n}}{d\xi} + T \cdot \frac{d^2C_{t,n}}{d\xi^2} \right) \tag{E.16}$$

$$\frac{dJ_{visc,n}}{d\xi} = \frac{-\Phi_n}{\mu} \left(C_{t,.n} \frac{d^2p_n}{d\xi} + \frac{dC_{t.n}}{d\xi} \frac{dp_n}{d\xi} \right) \tag{E.17}$$

$$-\frac{d\Phi_n}{d\xi} \cdot \frac{C_{t,n}}{\mu} \cdot \frac{dp}{d\xi} \tag{E.18}$$

$$\frac{dx_i}{d\xi} = \frac{d\left(\frac{C_{i,n}}{C_{t,n}}\right)}{d\xi} = \frac{\frac{dC_{i,n}}{d\xi} \cdot C_{t,n} - C_{i,n} \cdot \frac{dC_{t,n}}{d\xi}}{C_{t,n}^2} \tag{E.19}$$

$$\frac{dJ_{visc,i,n}}{d\xi} = x_{i,n} \frac{dJ_{visc,n}}{d\xi} + J_{visc,n} \cdot \frac{dx_{i,n}}{d\xi} \tag{E.20}$$

$$\frac{dJ^*_{diff,i,n}}{d\xi} = -D_{eff,i.n} \cdot \frac{d^2C_{i,n}}{d\xi^2} - \frac{dD_{eff,i,n}}{d\xi} \cdot \frac{dC_{i,n}}{d\xi} \tag{E.21}$$

$$\frac{dJ}{d\xi} = \sum_j \frac{dJ^*_{diff,j,n}}{d\xi} \tag{E.22}$$

$$\frac{dJ_{diff,i,n}}{d\xi} = \frac{dJ^*_{diff,i,n}}{d\xi} - \left(\frac{dx_{i,n}}{d\xi} \cdot J^*_{diff,n} + x_i \cdot \frac{dJ^*_{diff,n}}{d\xi} \right) \tag{E.23}$$

E.1.2. Derivatives for lsode

The following expressions were returned to the ODE solver lsode as function $f(\vec{Y}, t)$ in (E.1). For each gas species i in node n:

$$\frac{\partial C_{i,n\neq 0}}{\partial t} = \frac{1}{\phi} \left(\dot{\Gamma}_i - \frac{dJ_{visc,i,n}}{d\xi} - \frac{dJ_{diff,i,n}}{d\xi} \right) \tag{E.24}$$

$$\frac{\partial \rho_{char,n}}{\partial t} = -\left(R_{\mathrm{H_2O},n} + R_{\mathrm{CO_2},n} \right) \rho_{char,n} \tag{E.25}$$

$$\frac{\partial T_n}{\partial t} = 0 \tag{E.26}$$

The model was prepared for temperature variations, but temperatures were always kept constant at the initially chosen temperature with (E.26).

E.2. Program listings

This is the listing of the Octave/Matlab program used to model gasification of beech wood slabs:

```
%**************************************************************************
%*                                                                        *
%*    Slab model of wood gasification with CO2 and H2O                    *
%*                                                                        *
%*    Author: Claus Hindsgaul claush@mek.dtu.dk                           *
%*                                                                        *
%*    Part of Ph.D. study 2003-2006                                       *
%*                                                                        *
%**************************************************************************
%  Usage: pmodel13(nnodes, xlength,tend, Temp, orientation,
%               cH2O, cCO2, knudsen, fileid)
%  Orientation: "L", "R" or "T"
%  knudsen: If 1, Deff/D is corrected to assumed pure Knudsen
%            temperature dependence

% Version 13: Water gas shift
% Version 12: Corrective Jdiff element, variable porosity
% Version 10: Blancs diffusion coefficients and dDeffdxi1
% Version 9: Intermediate variable loop
% Version 8: Add N2 gas to all nodes

function modelresult = pmodel13(nnodes1, samplethickness, tend, Temp, or,
  cH2O, cCO2, knudsen0, fileid)

starttime=time;
global orientation;
orientation=or;
timespan=linspace(0,tend,200);
modelid="pm13";
printf("Model: %s_%s\n", modelid, fileid);
global NNODES;
NNODES=nnodes1;     %Number of nodes in the xi direction
global KNUDSEN;
KNUDSEN=knudsen0;
global dxi;
dxi = samplethickness/NNODES; %nodewidth [m]
global rhochar = 451.0; % Initial density of char [kg/m^3]
global Ru = 8.3144;    % Universal gas constant [J/(mol*K)]
Pambient = 101.3E3; # Ambient pressure [Pa]

# Binary diffusion coefficients at 673.15K:
# [Lide05], except:
# FSG-correlation: H2O-H2, H2O-CO
# [Marrero72]:N2-CO, N2-CO2
#
#                         N2      H2O     H2      CO      CO2
global Dijmatrix=1E-4*[  0,     0.720,  3.196,  0.863,  0.733; #N2
                         0.720, 0,      3.766,  1.084,  1.021; #H2O
```

```
                    3.196, 3.766,  0,      3.196,  2.745; #H2
                    0.863, 1.084,  3.196,  0,      0.546; #CO
        0.733, 1.021,  2.745,  0.546,  0   ]; #CO2


% Indices in each node
global I;
I.T = 0;          % Temperature [K]
I.rho = 1;        % Char density [kg/m^3]
I.cN2 =  I.firstgas= 2;       % Gas concentration N2
I.cH2O = 3;       % Gas concentration H2O
I.cH2 = 4;        % Gas concentration CH2
I.cCO = 5;         % Gas concentration CO
I.cCO2 = I.lastgas = 6;        % Gas concentration CO2

# Index to refer to all gases simultaneaously (vector operations)
I.gases = (I.firstgas:I.lastgas);


global NODESIZE = I.cCO2 +1;
global Neq=NNODES*NODESIZE;
Kall = 1+NODESIZE*(0:NNODES-1); % All node indices

global yambient=zeros(NODESIZE,1);
y0 = zeros(Neq,1);

y0(Kall+I.T)=Temp;   % [K]
y0(Kall+I.rho) = rhochar;   % [kg/m^3]
#initially soaked with N2 at atmospheric pressure
initialCt=Pambient./(Ru*y0(Kall+I.T)); % [mol/m^3]
y0(Kall+I.cN2)=initialCt;   % [mol/m^3]


# Ambient gas concentrations and temperature
global yambient=zeros(NODESIZE,1)
yambient(1+I.T)=Temp;
yambient(1+I.cH2O) = cH2O * Pambient./(Ru*yambient(1+I.T)); # Ambient H2O concentration [mol/m^3]
yambient(1+I.cCO2) = cCO2 * Pambient./(Ru*yambient(1+I.T)); # Ambient CO2 concentration [mol/m^3]
# Fill in with N2
yambient(1+I.cN2) = (1-cH2O-cCO2) * Pambient./(Ru*yambient(1+I.T)); # Ambient N2 concentration [mol/m^3]


lsode_options("absolute tolerance", 1E-4);
lsode_options("relative tolerance", 1E-4);
lsode_options("integration method", "bdf"); # Options: stiff, bdf, adams
[y,istate,msg] = lsode('f_resid', y0, timespan);


if (istate > 0)
  printf("Successful calculation: %s\n",msg)
else
  printf("lsode error: %s\n",msg)
```

```
endif


default_save_format="binary";
save(sprintf("%s_%sdata.octave", modelid, fileid), "y");

modelresult=y;

printf("*******This simulation completed in %.1f seconds**********\n",time-starttime)
endfunction


################################################################################
################################################################################
################## Solver routine defining dY/dt ###############################
################################################################################
################################################################################
################################################################################
function res = f_resid(y, t)

  global orientation;
  global NNODES;
  global KNUDSEN;
  global NODESIZE;
  global Neq;
  global Ru;
  global I;
  global dxi;
  global yinitial;
  global yambient;
  global rhochar;
  global Dijmatrix;

# Indicate progress by printing model time in seconds
printf("%.1f ",t);

  % All nodes indices
  % Properties in all nodes can be accessed on vector form as
  % y(Kall+I.property)   where I.property is e.g. I.T or I.cH2O
  % The length derivatives can be accessed the same way with
  % dxi1(Kall+I.property) and dxi2(Kall+I.property)
  Kall = 1+NODESIZE*(0:NNODES-1);
  res=zeros(Neq,1);

  % Length derivatives
  middlenodeeq=(NODESIZE+1):(Neq-NODESIZE);
  dxi1=dxi2=zeros(Neq,1);
  dxi1(middlenodeeq) = (y(middlenodeeq+NODESIZE)\
       -y(middlenodeeq-NODESIZE))/(2*dxi);

  % Second length derivatives
  dxi2(middlenodeeq) = (y(middlenodeeq+NODESIZE)\
```

```
    +y(middlenodeeq-NODESIZE)\
    -2*y(middlenodeeq))/(dxi*dxi);

  % Length derivatives for node 1
  C=(1:NODESIZE);
  dxi1(C) = (y(C+NODESIZE)-yambient(C))/(2*dxi);
  dxi2(C) = (y(C+NODESIZE)+yambient(C)-2*y(C))/(dxi*dxi);


  % Length derivatives for last (inner) node
  C=((NNODES-1)*NODESIZE+1):(NNODES*NODESIZE);
  dxi1(C) = 0;
  dxi2(C) = (2*y(C-NODESIZE)-2*y(C))/(dxi*dxi);


  % Degree of conversion for all nodes
  X=1-y(Kall+I.rho)/rhochar;

  % Beechreactivity needs partial pressures Pi in [atm]
  % Calculate factors to multiply the [mol/m^3] concentrations to
  % get Pi [atm] partial pressures;
  % pi = Ci*Ru*T
  RT=Ru*y(Kall+I.T)/101.3E3;

  %reactivities for all nodes
   re=beechreactivity(y(Kall+I.T),X,\
     y(Kall+I.cH2O).*RT, y(Kall+I.cH2 ).*RT,\
     y(Kall+I.cCO ).*RT, y(Kall+I.cCO2).*RT); % [1/s]

  % Total gas concentration and derivatives for all nodes
  Ct=dCtdxi1=dCtdxi2=zeros(NNODES,1);
  for gas=I.firstgas:I.lastgas;
    Ct=Ct+y(Kall+gas);      # Total conc [mol/m^2]
    dCtdxi1=dCtdxi1+dxi1(Kall+gas);  # First length derivative of total conc [mol/m^5]
    dCtdxi2=dCtdxi2+dxi2(Kall+gas);  # Second length derivative of total conc [mol/m^5]
  endfor

% Pressure derivatives
dpdxi1 = Ru*(dxi1(Kall+I.T).*Ct+y(Kall+I.T).*dCtdxi1);
dpdxi2 = Ru*(dxi2(Kall+I.T).*Ct+2*dxi1(Kall+I.T).*dCtdxi1+y(Kall+I.T).*dCtdxi2);

%Gas diffusivities
DeD=Phi=dPhidxi1=zeros(NNODES,1);
Deffi=dDeffdxi1=dDeffidxi2=zeros(NNODES,I.lastgas-I.firstgas+1);

if(orientation == "L")
  DeD = 0.484+0*X;                      % Deff/Dij longitudinal
  Phi=16000+0*X;                       % Permeability [mD]
elseif(orientation == "R")
  DeD = 0.00126*exp(9.31*X);          % Deff/Dij radial
  K0pt = 1.37E-9*exp(9.31*X);          % K0*phi/tau [m]
  Phi=0.226*exp(8.56*X+9.3*X.*X);      % Permeability [mD]
```

```
elseif(orientation == "T")
  DeD = 0.00062*exp(6.0*X+4.8*X.*X); % Deff/Dij tangential
  K0pt = 0.67E-9*exp(6.02*X+4.8*X.*X);   % K0*phi/tau [m]
  Phi=0.720*exp(-2.51*X+16.2*X.*X);     % Permeability [mD]
 else
    error(sprintf("Unknown orientation: %s",orientation));
endif

#Local porosity
porosity=0.7+0.3*X;

DeD = min(DeD,0.484); # Assumption: Deff/D never exceeds that of the L direction
Phi = min(Phi,16000); # Permeability never exceeds that of the L direction


% Viscosities (based on N2 at 600K, [Lide06]) [Pa*s]
mu=29.6E-6*sqrt(y(Kall+I.T)/600);

% Viscous flux
Jvisc= -(Ct.*(Phi*1E-15)./mu).*dpdxi1;

Dijb=zeros(NNODES,I.lastgas-I.firstgas+1);  # Blancs (ordinary) diffusion coefficient
DeffiK=zeros(NNODES,I.lastgas-I.firstgas+1); # Knudsen diffusion coefficients

### Loop through nodes for Blancs law diffusion coefficients ################################
for k = 1:NNODES; %*************** LOOP THROUGH ALL NODES

  C = (k-1)*NODESIZE+1; % node index base for node k

#     N2     H2O     H2     CO    CO2
  Mi=[28.01, 18.01, 2.01, 28.01, 44.01]; # Gas molar masses

# Calculate Blancs diffusion coefficients:
    for gas = ((I.firstgas:I.lastgas)-I.firstgas+1);
      invDijb = (y(C+I.gases)/Ct(k))./Dijmatrix(:,gas);
      invDijb(gas)=0; # Exclude gas i=gas
      invDijb=sum(invDijb);
     if(invDijb!=0)
       Dijb(k,gas)=(1-y(C+gas+I.firstgas-1)/Ct(k))*((y(C+I.T)/673.15)^1.75).*(1/invDijb);
     else #No other gases in mixture, self-diffusion Dijb=1.0E-4
       Dijb(k,gas)=((y(C+I.T)/673.15)^1.75)*1.0E-4;
     endif
     if(KNUDSEN) #Knudsen diffusion coefficient
DeffiK(k,gas)=(4/3)*K0pt(k).*sqrt((8*Ru*y(C+I.T))./(pi*Mi(gas)));
      endif
    endfor
% Ordinary diffusivity for all I.gases in node k [m^2/s]
    DeffiB(k,:) = DeD(k)*Dijb(k,:); #Blancs (ordinary) diffusion coefficient
  endfor

if(KNUDSEN)
  Deffi=DeffiK;
```

```
else
  Deffi=DeffiB;
endif

# First length derivative of Deffi and Phi
   middlenodes = (2:(NNODES-1));
   dDeffidxi1(middlenodes,:) = (Deffi(middlenodes+1,:)-Deffi(middlenodes-1,:))/(2*dxi);
   dDeffidxi1(1,:)=(Deffi(2,:)-Deffi(1,:))/dxi;
   dDeffidxi1(NNODES,:)=0;


   dPhidxi1(middlenodes) = (Phi(middlenodes+1)-Phi(middlenodes-1))/(2*dxi);
   dPhidxi1(1)=(Phi(2)-Phi(1))/dxi;
   dPhidxi1(NNODES)=0;

% Total viscous flux derivatives:
    dJvisctdxi1=-((Phi*1E-15)./mu).* \
      (Ct.*dpdxi2+dCtdxi1.*dpdxi1) \
       -(dPhidxi1*1E-15).*Ct.*dpdxi1./mu;

% Water gas shift  H2O + CO <-> CO2 + H2
   Ka=(1.303E-6*y(Kall+I.T)+7.17E-4).*y(Kall+I.T)-1.3006;
% Reactivity for water gas shift (rate constant=1 s^-1)
   reWGS=1*(y(Kall+I.cH2O).*y(Kall+I.cCO)./Ka \
            -y(Kall+I.cH2).*y(Kall+I.cCO2));
   reWGS(isnan(reWGS) | isinf(reWGS))=0;

### Loop for solver results ########################################
  for k = 1:NNODES; %**************** LOOP THROUGH ALL NODES
    C = (k-1)*NODESIZE+1; % node index base for node k

% re.CO2: C + CO2 -> 2CO
% re.H2O: C + H2O -> CO + H2
% reWGS: H2O + CO <-> CO2 + H2
    molprod=zeros(NODESIZE,1);
#     N2 H2O H2 CO CO2
    molprod(I.gases)= \
    ([ 0, 0, 0, 2,-1].*re.CO2(k)  \
    +[ 0,-1, 1, 1, 0].*re.H2O(k)) \
    .*(y(C+I.rho)/12) \
    +[ 0,-1, 1,-1, 1].*reWGS(k); % [mol/(m^3*s)]


% Mole fraction length deriviatives (dx_i/dxi):
    dxdxi1=(dxi1(C+I.gases).*Ct(k)-y(C+I.gases).*dCtdxi1(k))/(Ct(k)*Ct(k));

% Viscous flux of specie i derivatives:
     dJviscidxi1=(y(C+I.gases)/Ct(k)).*dJvisctdxi1(k) + Jvisc(k).*dxdxi1;

if(KNUDSEN)  # No correction needed
  dJdiffidxi1=-Deffi(k,:)'.*dxi2(C+I.gases) \
                -dDeffidxi1(k,:)'.*dxi1(C+I.gases);
```

```
else # Correction for Blanc flow
# Diffusion flux of specie i (Blancs approximation)
     JdiffiBlanc=-Deffi(k,:)'.*dxi1(C+I.gases);
# Diffusion flux derivative of specie i (Blancs approximation)
     dJdiffiBlancdxi1=-Deffi(k,:)'.*dxi2(C+I.gases) \
                 -dDeffidxi1(k,:)'.*dxi1(C+I.gases);
  # Corrective bulk flux derivative to restore zero bulk diffusion flux
  JdiffBlancCorrection=sum(JdiffiBlanc);
  dJdiffBlancCorrectiondxi1=sum(dJdiffiBlancdxi1);
  # Corrected diffusion flux derivative for specie i
  dJdiffidxi1 = dJdiffiBlancdxi1-(dxdxi1*JdiffBlancCorrection \
  +(y(C+I.gases)/Ct(k))*dJdiffBlancCorrectiondxi1);
endif

     res(C+I.gases)=(molprod(I.gases)-dJviscidxi1-dJdiffidxi1)/porosity(k);

  endfor  % *************** END LOOP THROUGH ALL NODES

  res(Kall+I.rho)  = (-(re.H2O+re.CO2).*y(Kall+I.rho));

  % Keep Temperature constant
  res(Kall+I.T)    = 0;

endfunction
```

Beech char reactivity subroutine:

```
function R_beech = beechreactivity(T,x,pH2O,pH2,pCO,pCO2)
  ## Usage: beech_reactivity(T, pH2O, pH2, pCO, pCO2)
  ## T is temperature in [K] (valid 1023-1273K)
  ## pH2O, pH2, pCO, pCO are partial pressures [atm]
  ## Calculate the reactivity of beech char
  ## using Benny Gøbels reactivity expression

  x = min(x,0.8); # Assume re(x>0.8)=re(x=0.8)

  Ru = 8.3144; # [J/(mol*K)]
  k1 = 7.531E7*exp(-2.11E5./(Ru*T)); # [1/(s*atm)]
  k2 = 3.270E8*exp(-2.48E5./(Ru*T)); # [1/(s*atm)]
  k3 = 3.282E6*exp(-1.52E5./(Ru*T)); # [1/(s*atm)]
  k4 = 2.016E8*exp(-2.17E5./(Ru*T)); # [1/(s*atm)]
  k5 = 2.458E7*exp(-2.14E5./(Ru*T)); # [1/(s*atm)]

  f = (378.10*x.^6 -707.17*x.^5 +504.22*x.^4
       -166.33*x.^3 +25.333*x.^2 -0.61855*x  +0.44280);

# Low H2O, high H2 expression
#  f = (32.174*x.^6 -57.172*x.^5 +46.096*x.^4
#       -16.043*x.^3 +2.924*x.^2 -0.2972*x  +0.5286);

  denominator=(1+(k1./k5).*pH2O+(k2./k5).*pCO2 \
       +(k3./k5).*pH2+(k4./k5).*pCO);

    R_beech.H2O=f.*(k1.*pH2O) \
      ./denominator; # 1/s

    R_beech.CO2=f.*(k2.*pCO2) \
      ./denominator; # 1/s

endfunction
```

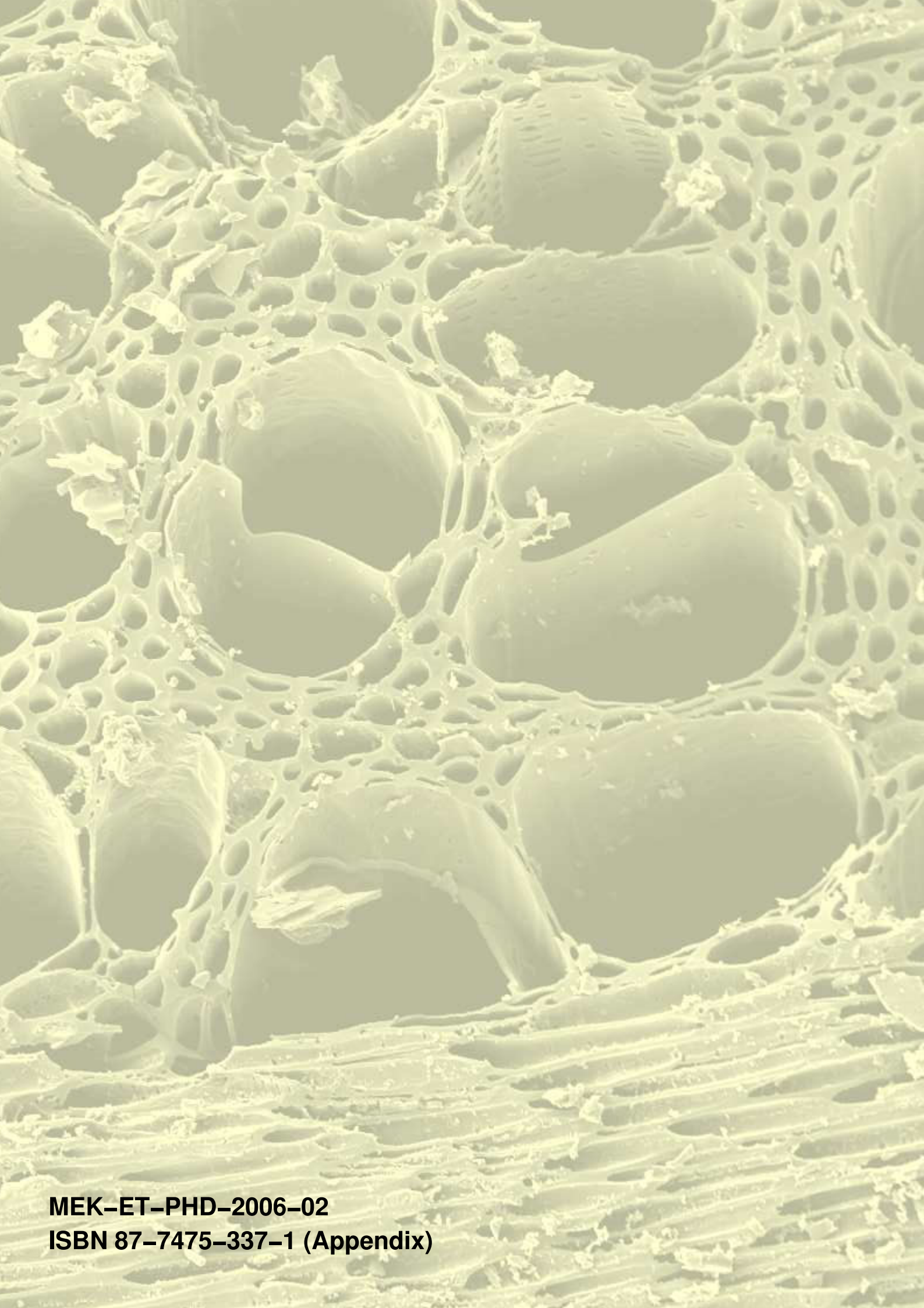

MEK–ET–PHD–2006–02
ISBN 87–7475–337–1 (Appendix)